# SUPERSOLAR METALLICITY IN WEAK Mg II ABSORPTION SYSTEMS AT $z \sim 1.7$[1]

Toru Misawa,[2] Jane C. Charlton,[2] and Anand Narayanan[2]
Received 2007 June 20; accepted 2008 January 7

## ABSTRACT

Through photoionization modeling, constraints on the physical conditions of three $z \sim 1.7$ single-cloud weak Mg II systems $[W_r(2796) \leq 0.3$ Å$]$ are derived. Constraints are provided by high-resolution $R = 45,000$, high-S/N spectra of the three quasars HE 0141−3932, HE 0429−4091, and HE 2243−6031, which we have obtained from the ESO archive of VLT UVES. Results are as follows: (1) The single-cloud weak Mg II absorption in the three $z \sim 1.7$ systems is produced by clouds with ionization parameters of $-3.8 < \log U \lesssim -2.0$ and sizes of 1–100 pc. (2) In addition to the low-ionization phase Mg II clouds, all systems need an additional one to three high-ionization phase C IV clouds within 100 km s$^{-1}$ of the Mg II component. The ionization parameters of the C IV clouds range from $-1.9 < \log U < -1.0$, with sizes of tens of parsecs to kiloparsecs. (3) Two of the three single-cloud weak Mg II absorbers have near-solar or supersolar metallicities, if we assume a solar abundance pattern. Although such large metallicities have been found for $z < 1$ weak Mg II absorbers, these are the first high metallicities derived for such systems at higher redshifts. (4) Two of the three weak Mg II systems also need additional low-metallicity, broad Ly$\alpha$ absorption lines, offset in velocity from the metal-line absorption, in order to reproduce the full Ly$\alpha$ profile. (5) Metallicities in single-cloud weak Mg II systems are more than an order of magnitude larger than those in DLA systems at $z \sim 1.7$. In fact, there appears to be a gradual decrease in metallicity with increasing $N_{\rm H\,I}$, from these, the most metal-rich Ly$\alpha$ forest clouds, to Lyman limit systems, to sub-DLAs, and finally to the DLAs.

*Subject headings:* galaxies: abundances — intergalactic medium — quasars: absorption lines — quasars: individual (HE 0141−3932, HE 0429−4901, HE 2243−6031)

*Online material:* color figures

## 1. INTRODUCTION

Many single-cloud weak Mg II absorbers $[W_r(2796) \leq 0.3$ Å$]$ at $0.4 < z < 1.0$ have been found to have solar or even super-solar metallicities (Rigby et al. 2002; Charlton et al. 2003). This is quite puzzling in view of the fact that they tend to be found at distances of 40–100 kpc from star-forming galaxies (Churchill et al. 2005; Milutinović et al. 2006), and not near detected sites of star formation. These objects have a cross section similar to the absorption cross section of luminous galaxies, and thus they occupy a significant volume of the universe (Rigby et al. 2002). Because weak Mg II systems only contain a small mass, they do not trace the cosmic metal abundance. Nevertheless, it is still important to understand local star formation activities in the full range of environments over cosmic time.

Narayanan et al. (2007) presented the results of a search for weak Mg II absorption in Very Large Telescope (VLT) UVES quasar spectra over a cumulative redshift path of 77.3 at $0.4 < z < 2.4$. A total of 116 Mg II absorbers with $0.02$ Å $< W_r(2796) < 0.3$ Å were detected, with ∼60% of these having just a single-cloud, narrow component in Mg II. It has been argued that a large fraction of the population of multiple-cloud weak Mg II absorbers (i.e., absorbers with multiple clouds that are resolved by high-resolution $[R \sim 40,000]$ spectroscopies) have a different physical origin from the single-cloud weak Mg II absorbers (Rigby et al. 2002; Masiero et al. 2005; Ding et al. 2005). Narayanan et al. (2007) found that the redshift path density, $dN/dz$, of weak Mg II absorbers increases from $z = 2.4$ to 1.2, where it peaks, and subsequently declines until the present.

Narayanan et al. (2007) followed a weak Mg II survey of Lynch et al. (2006), which used a small subset of high-quality VLT UVES quasar spectra. From that survey, Lynch & Charlton (2007) selected the nine $z > 1.4$ weak Mg II absorbers and applied photoionization models. Of these, four were single-cloud weak Mg II absorbers with coverage of the corresponding Ly$\alpha$ transitions, so that metallicities could be constrained.

In general, Lynch & Charlton (2007) found that the physical conditions of the $z > 1.4$ weak Mg II absorbers were similar to those of the same class of absorbers at lower redshift, suggesting that the same production mechanisms are responsible over this time period. However, in contrast to the situation at low redshift (Rigby et al. 2002; Charlton et al. 2003), Lynch & Charlton (2007) were only able to derive lower limits to the metallicity, ranging from 1/100 to 1/10 of the solar value. Single-cloud weak Mg II absorbers, in addition to the cloud that produced the Mg II absorption, have separate, lower density C IV clouds that are spread over tens to hundreds of kilometers per second (Charlton et al. 2003; Lynch & Charlton 2007). The reason that only lower limits could be derived for the metallicity in these cases was because of the contributions to the Ly$\alpha$ profile from the kinematically spread C IV clouds. On the other hand, Lynch & Charlton (2007) also suggested that there could be a buildup of metals in the population of single-cloud weak Mg II absorbers from $z = \sim 2$ to ∼0.4.

In view of the large spread of metallicity constraints at any redshift, a sample of only four $z > 1.4$ single-cloud weak Mg II absorbers was not sufficient to resolve the issue of whether metallicity evolution occurs in the population. We therefore identified three additional $z > 1.4$ candidates for photoionization modeling from the larger survey of Narayanan et al. (2007). These systems, the $z = 1.78169$ absorber toward HE 0141−3932, the $z = 1.68079$ absorber toward HE 0429−4091, and the $z = 1.75570$ absorber toward HE 2243−6031, have high signal-to-noise ratio (S/N) VLT UVES coverage of key constraining metal-line transitions,

| QSO (1) | R.A. (2) | Decl. (3) | $z_{em}$ (4) | $m_V$ (mag) (5) | $\lambda^a$ (Å) (6) | Setting[b] (7) | $t_{exp}$ (s) (8) | Date (9) | Prog. ID[c] (10) |
|---|---|---|---|---|---|---|---|---|---|
| HE 0141−3932......... | 01 43 33.70 | −39 17 01.0 | 1.807 | 16.3 | 3060–10000 | 437 × 860 | 14,400 | 2001 Jul 19–Aug 24 | 67.A-0280 |
| | | | | | | 346 × 580 | 25,200 | | |
| HE 0429−4901.......... | 04 30 37.39 | −48 55 24.2 | 1.940 | 16.2 | 3050–10080 | 437 × 860 | 18,835 | 2001 Jan 13–Mar 19 | 66.A-0221 |
| | | | | | | 346 × 580 | 10,800 | | |
| HE 2243−6031........... | 22 47 08.85 | −60 15 46.9 | 3.010 | 18.3 | 3140–10000 | 346 × 580 | 14,400 | 2000 Jun 4–Jun 12 | 65.O-0411 |
| | | | | | | 437 × 860 | 11,400 | | |

Note.—Units of right ascension are hours, minutes, and seconds, and units of declination are degrees, arcminutes, and arcseconds.
[a] Observed wavelength range.
[b] Central wavelength for blue and red CCD chips of VLT UVES.
[c] Proposal ID used at the ESO Web site.

as well as Lyα. We apply Cloudy (Ferland et al. 1998) photo-ionization models to constrain the ionization parameters and metallicities of the phases[3] of gas that are required to fit the data. Our focus is on the question of the metallicity evolution of the single-cloud weak Mg II absorbers and on comparing the result to the metallicity evolution of other classes of quasar absorption-line systems.

We begin in § 2 with a summary of the data that we have used to constrain the properties of the three $z \sim 1.7$ single-cloud weak Mg II absorbers. Next, in § 3, we describe our procedure for photoionization modeling with Cloudy, which is based on comparing synthetic model profiles to the data. Section 4 presents the detailed results for the three absorbers. Finally, in § 5, we summarize those results, compare the metallicities of single-cloud weak Mg II absorbers to damped Lyα systems (DLAs), to sub-DLAs, and to Lyman limit absorbers, and discuss the implications of this comparison. Throughout this paper we use a cosmology with $H_0 = 72$ km s$^{-1}$ Mpc$^{-1}$, $\Omega_m = 0.3$, and $\Omega_\Lambda = 0.7$.

## 2. DATA

All three weak Mg II systems in our sample were found in the survey of Narayanan et al. (2007), who studied the statistical properties of weak Mg II systems using 81 VLT UVES spectra. Data were retrieved from the ESO archive and reduced using the ESO MIDAS pipeline. In the case of multiple epoch observations, the individual exposures were combined to enhance the S/N. The detailed description of the original data analysis is presented in Narayanan et al. (2007).

The main purpose of this paper is to place strict constraints on physical properties (such as metallicity, ionization parameter,[4] gas temperature, and size) of single-cloud, weak Mg II absorbers at high redshift. Among the 116 weak Mg II systems in Narayanan et al. (2007), 16 systems at relatively high redshift ($z > 1.5$) have Lyα absorption lines covered with the observed spectra. Lyα is quite important for determining metallicities. Of the 16 systems, 7 are classified as single-cloud systems. Four of these 7, the $z = 1.65146$ system toward HE 0001−2340, the $z = 1.70849$ system toward HE 0151−4326, the $z = 1.79624$ system toward HE 2347−4342, and the $z = 2.17455$ system toward HE 0940−1050, had already been modeled, as described in Lynch & Charlton (2007), since they were first identified in the earlier survey of Lynch et al. (2006). The other three systems, the $z = 1.78169$ system toward

HE 0141−3932, the $z = 1.68079$ system toward HE 0429−4091, and the $z = 1.75570$ system toward HE 2243−6031, are modeled in the present paper.

In Table 1 we give an observation log for the three quasars toward which the single-cloud weak Mg II absorbers were detected. Column (1) is the quasar name, columns (2) and (3) are the coordinates of the quasars, columns (4) and (5) are the emission redshift and optical magnitude of the quasars, column (6) is observed wavelength range, column (7) is the central wavelength for the blue and red CCDs of VLT UVES, columns (8) and (9) are total exposure time and observing date, and column (10) is the proposal identification. By chance, all three quasars were observed as part of programs with the same PI, Sebastian Lopez.

The absorption profiles for key transitions used to constrain the three single-cloud weak Mg II absorbers are displayed in Figures 1, 2, and 3. Rest-frame equivalent widths and 5 σ rest-frame equivalent width limits for these same transitions are listed in Table 2.

## 3. PHOTOIONIZATION MODELS

In this section we briefly summarize the strategy for photoionization modeling, which is similar to the procedure practiced in previous studies (e.g., Churchill & Charlton 1999; Charlton et al. 2003; Lynch & Charlton 2007). At first, we determine the line parameters (column density, Doppler parameter, and redshift) for the Mg II doublets, using a Voigt profile fitting code (MINFIT; Churchill et al. 2003). For each of the three absorbers modeled here, a single absorption component provided an adequate fit to the Mg II doublet. The best-fit parameters are listed in Table 3: column (1) is the name of the transition, columns (2), (3), and (4) are the fit parameters of velocity shift from the system central redshift,[5] column density, and Doppler parameter with their 1 σ errors. For completeness, we also applied formal Voigt profile fits to other detected transitions, and listed the results in Table 3. We emphasize, however, that we did not use these values (except for the optimized transitions) to determine model constraints. Instead, we compared directly to the shapes of the observed absorption profiles as described below.

Assuming that the absorbing clouds are in photoionization equilibrium, their ionization conditions are derived using the photoionization code Cloudy, version 07.02.00 (Ferland et al. 1998), optimizing on the observed column density of Mg II and comparing model predictions to other observed low-ionization transitions. The clouds in each phase are modeled as plane-parallel

---

[3] Phases are defined as regions of gas with similar metallicity, temperature, and volume density.
[4] The ionization parameter is defined the ratio of ionizing photons ($n_\gamma$) to the number of hydrogen in the absorbing gas ($n_H$).

[5] The system central redshift is defined as the flux-weighted center of the Mg II λ2796 absorption line.
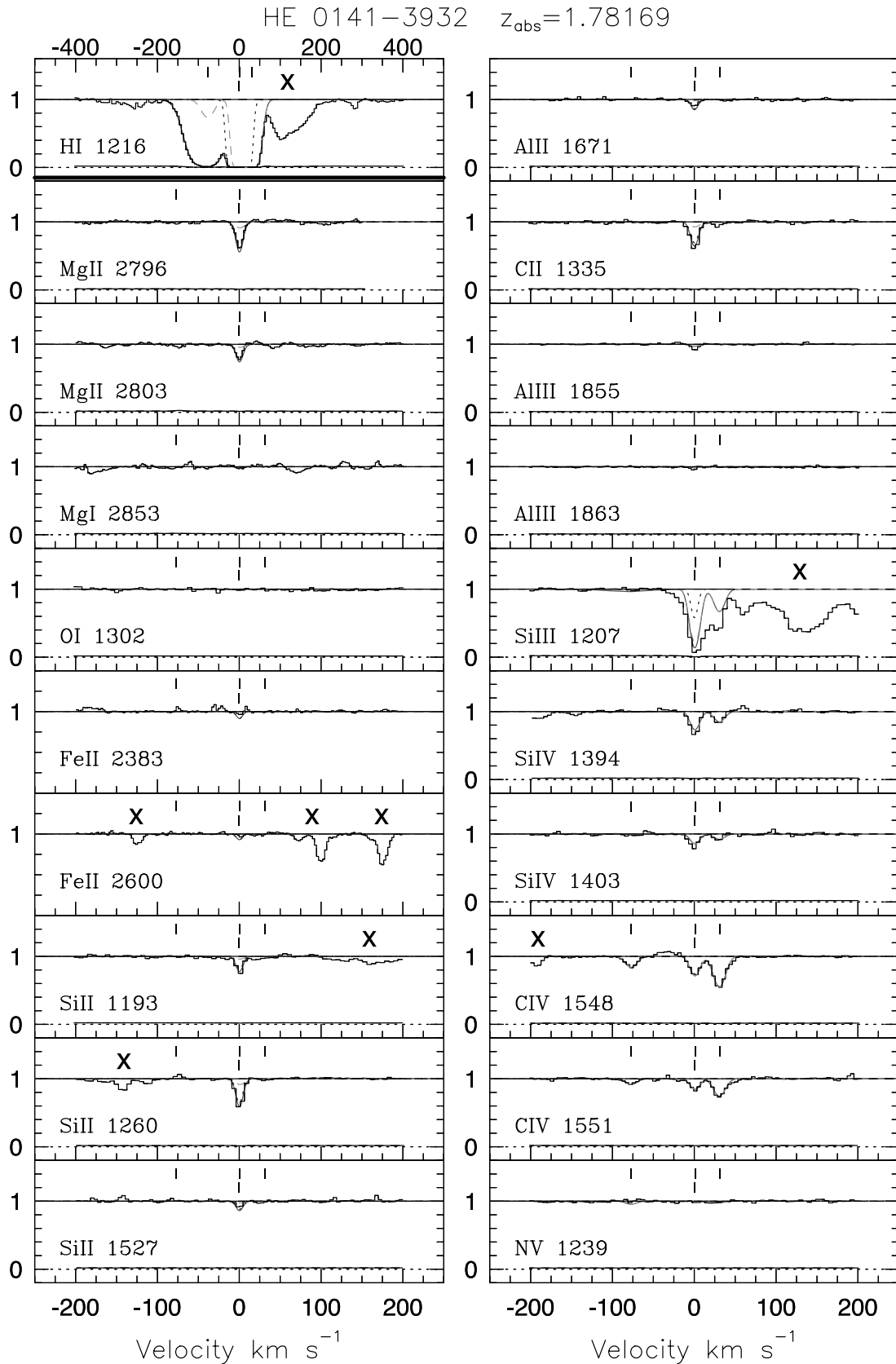
FIG. 1.—Detected transitions and those that provide limiting constraints, shown in velocity space for the single-cloud weak Mg II system at $z = 1.78169$ toward HE 0141−3932. The velocity range is $\pm 200$ km s$^{-1}$ for all transitions except for Ly$\alpha$ whose range is $\pm 400$ km s$^{-1}$. The vertical scale is from $-0.2$ to 1.6, except for Fe II $\lambda 2383$ and Fe II $\lambda 2600$ for which it is slightly zoomed from 0.2 to 1.4. The data are from a VLT UVES spectrum with a resolution of $R = 45,000$. The $\sigma$ spectrum is indicated as a solid histogram just above the dotted line crossing each plot at zero flux. Features from unrelated systems are marked with a cross. An example of the best model fit to the observed spectrum (summarized in Table 6) is superimposed on the data as a solid curve. Contributions of the Mg II and C IV clouds to the model are displayed separately as dotted and long-dashed lines. A single tick centered on the Mg II profile marks the position of the low-ionization phase, while ticks in the row above mark the positions of the high-ionization phase clouds. [*See the electronic edition of the Journal for a color version of this figure.*]
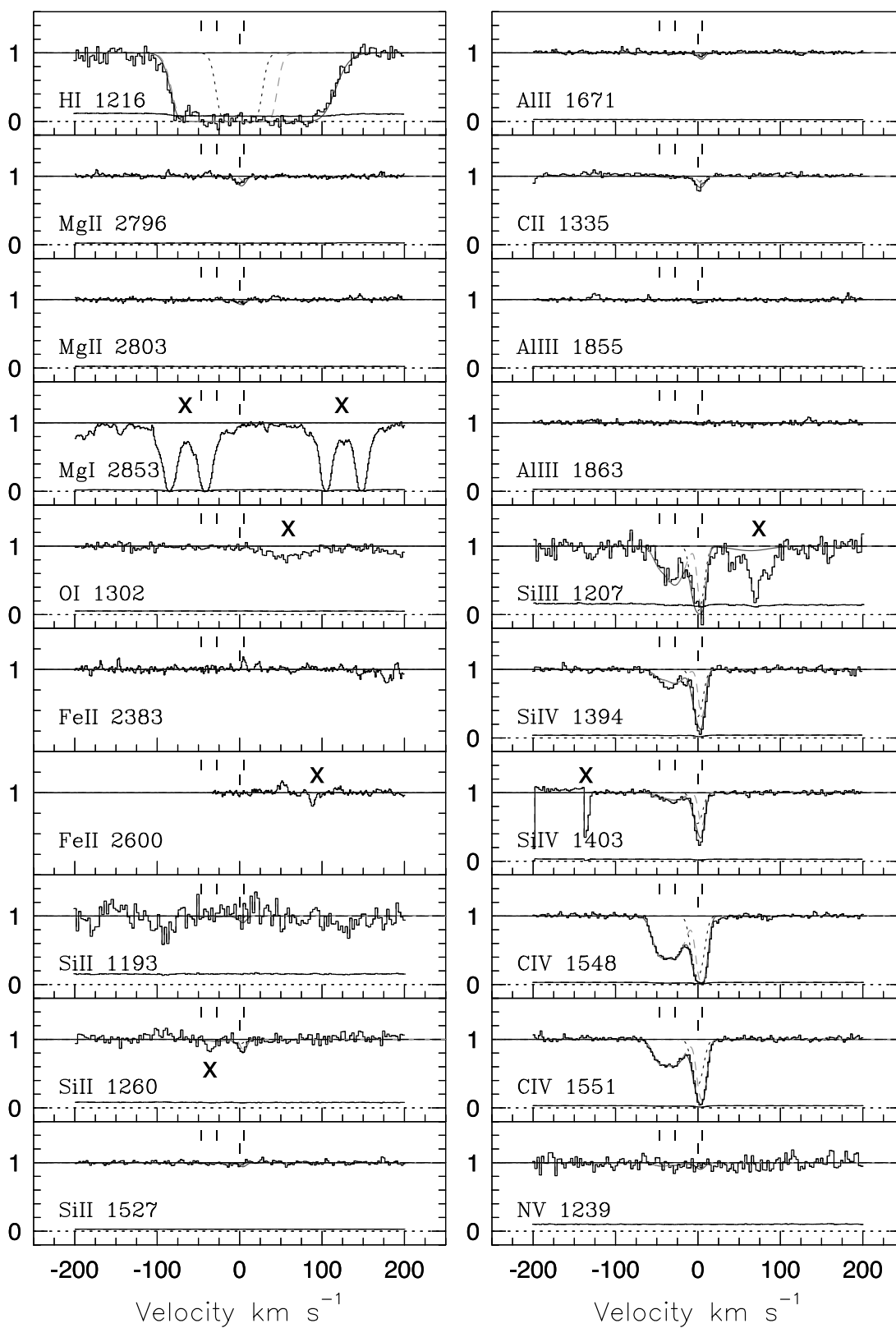
HE 0429−4091   $z_{abs}$=1.68079

Fig. 2.—Same as Fig. 1, but for the system at $z = 1.68079$ toward HE 0429−4901. [*See the electronic edition of the Journal for a color version of this figure.*]
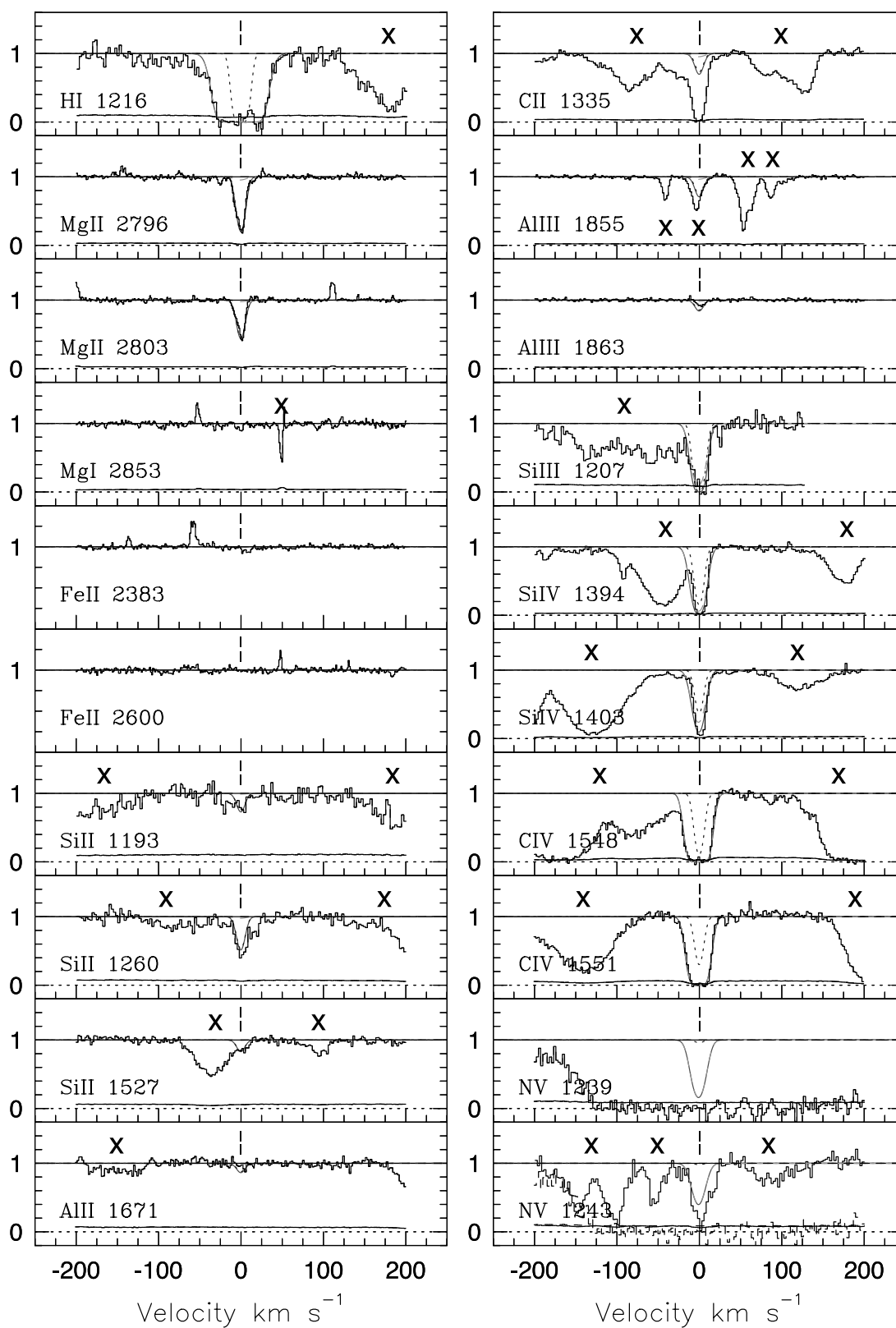
FIG. 3.—Same as Fig. 1, but for the system at $z = 1.75570$ toward HE 2243−6031. [*See the electronic edition of the Journal for a color version of this figure.*]

TABLE 2
REST-FRAME EQUIVALENT WIDTHS

| | EQUIVALENT WIDTH, $W_{rest}$ (Å)[a] | | |
|---|---|---|---|
| TRANSITION | System 1 ($z_{abs} = 1.78169$) | System 2 ($z_{abs} = 1.68079$) | System 3 ($z_{abs} = 1.75570$) |
| Ly$\alpha$........................... | $0.991 \pm 0.003$ | $0.816 \pm 0.009$ | $0.341 \pm 0.008$ |
| Mg II $\lambda2796$ ........... | $0.039 \pm 0.001$ | $0.015 \pm 0.001$ | $0.121 \pm 0.003$ |
| Mg II $\lambda2803$ ........... | $0.020 \pm 0.001$ | $0.008 \pm 0.001$ | $0.059 \pm 0.001$ |
| Mg I $\lambda2853$ ............. | $<0.001$ | $<0.001^{b}$ | $0.007 \pm 0.001$ |
| O I $\lambda1302$ ................ | $<0.001$ | $<0.001$ | $<0.147^{b}$ |
| Fe II $\lambda2383$ .............. | $<0.001$ | $<0.001$ | $0.009 \pm 0.002$ |
| Fe II $\lambda2600$ .............. | $0.002 \pm 0.001$ | $<0.001$ | $<0.001$ |
| Si II $\lambda1193$ .............. | $0.018 \pm 0.002$ | $<0.003$ | $\sim0.015^{b}$ |
| Si II $\lambda1260$ .............. | $0.020 \pm 0.001$ | $0.008 \pm 0.002$ | $\sim0.040^{b}$ |
| Si II $\lambda1527$ .............. | $0.004 \pm 0.001$ | $<0.001$ | $\sim0.019^{b}$ |
| Al II $\lambda1671$ .............. | $0.006 \pm 0.001$ | $0.003 \pm 0.001$ | $<0.002$ |
| C II $\lambda1335$ .............. | $0.028 \pm 0.001$ | $0.012 \pm 0.001$ | $<0.438^{b}$ |
| Al III $\lambda1855$ .............. | $0.004 \pm 0.000$ | $0.005 \pm 0.001$ | $<0.045^{b}$ |
| Al III $\lambda1863$ .............. | $0.002 \pm 0.000$ | $<0.001$ | $0.006 \pm 0.001$ |
| Si III $\lambda1207$.............. | $<0.147^{b}$ | $0.114 \pm 0.008$ | $0.101 \pm 0.004$ |
| Si IV $\lambda1394$.............. | $0.032 \pm 0.002$ | $0.110 \pm 0.002$ | $0.100 \pm 0.001$ |
| Si IV $\lambda1403$.............. | $0.019 \pm 0.002$ | $0.069 \pm 0.002$ | $0.081 \pm 0.001$ |
| C IV $\lambda1548$ .............. | $0.082 \pm 0.002$ | $0.250 \pm 0.002$ | $0.196 \pm 0.002$ |
| C IV $\lambda1551$ .............. | $0.048 \pm 0.002$ | $0.171 \pm 0.002$ | $0.174 \pm 0.003$ |
| N V $\lambda1239$ .............. | $<0.001$ | $<0.002$ | c |

[a] Errors include both photon noise and continuum level uncertainty.
[b] Blending with other lines.
[c] Flux is completely black.

structures of constant density. The ionization parameter [$\log U = \log (n_\gamma/n_H)$] and metallicity ($Z/Z_\odot$) of the clouds serve as free parameters in the modeling. The elemental abundance pattern is initially assumed to be solar, and variations are explored when they are suggested by the data.

Following Haardt & Madau (1996); Haardt & Madau (2001) we take the combined flux from quasars and star forming galaxies at $z \sim 1.7$ (with a photon escape fraction of 0.1) as an extragalactic background radiation (i.e., incident flux on the absorbers). We consider the possible effects of a nearby stellar contribution to the ionizing radiation field in § 4.4, although it should be safe to ignore them, since weak Mg II absorbers are not often within 40 kpc of bright galaxies (Rigby et al. 2002; Churchill et al. 2005).

The metallicity and ionization parameter are initially varied in steps of 0.5 dex, and then fine-tuned to select the model that corresponds best with the observed data in steps of 0.1 dex. The column densities for various ionization stages of each element and the equilibrium gas temperature are provided by the Cloudy model. The Doppler parameter for each element can then be calculated from the expression for total line width, $b_{tot}^2 = b_{ther}^2 + b_{turb}^2$, where $b_{ther}$ [$= (2kT/m)^{1/2}$] is the thermal contribution to the line width corresponding to a gas temperature $T$ and $b_{turb}$, the contribution from internal gas turbulence. This latter quantity, which is uniform across elements, is estimated using the gas temperature from the Cloudy model and the observed Doppler parameter of the element on which the model is optimized. From the derived column densities and Doppler parameters, a synthetic spectrum is generated and compared to the observed spectrum after convolving with a Gaussian instrumental spread function ($R = 45,000$ in the case of our VLT UVES spectra).

Although the observed and the synthesized spectra are compared by eye, the method generally gives good results in the sense that other models whose metallicity and ionization parameter are (sometimes only slightly) different than the best values would make the

TABLE 3
VOIGT PROFILE FITS FOR DETECTED TRANSITIONS

| Transition (1) | $\Delta v$ (km s$^{-1}$) (2) | $\log N$ (3) | $b$ (km s$^{-1}$) (4) | Optimized[a] (5) |
|---|---|---|---|---|
| $z = 1.78169$ (HE 0141$-$3932) | | | | |
| H I ................ | $-82$ | $>14.36^{b}$ | $42.3 \pm 0.3$ | x |
| | $11$ | $>15.28^{b}$ | $21.5 \pm 0.5$ | |
| Mg II............. | $0$ | $12.05 \pm 0.01$ | $4.1 \pm 0.2$ | x |
| Fe II ............. | $2$ | $11.29 \pm 9.99$ | $1.1 \pm 99.9$ | |
| Si II .............. | $0$ | $12.26 \pm 0.01$ | $4.5 \pm 0.3$ | |
| Al II .............. | $0$ | $11.16 \pm 0.07$ | $5.6 \pm 1.5$ | |
| C II .............. | $0$ | $13.16 \pm 0.01$ | $5.6 \pm 0.3$ | |
| | $28$ | $12.33 \pm 0.08$ | $6.4 \pm 1.9$ | |
| Al III ............ | $0$ | $11.51 \pm 0.04$ | $3.4 \pm 0.9$ | |
| Si IV ............ | $0$ | $12.46 \pm 0.02$ | $6.0 \pm 0.4$ | |
| | $29$ | $12.11 \pm 0.04$ | $5.8 \pm 0.9$ | |
| C IV .............. | $-77$ | $12.57 \pm 0.03$ | $8.7 \pm 0.9$ | x |
| | $1$ | $12.80 \pm 0.02$ | $7.4 \pm 0.4$ | x |
| | $31$ | $13.13 \pm 0.01$ | $9.0 \pm 0.3$ | x |
| $z = 1.68079$ (HE 0429$-$4091) | | | | |
| H I ................ | $14$ | $>15.57^{b}$ | $48.3 \pm 2.3$ | |
| | $(64)^{c}$ | $(>14.6)^{c}$ | $(34)^{c}$ | x |
| Mg II............. | $0$ | $11.52 \pm 0.09$ | $6.9 \pm 2.3$ | x |
| Si II .............. | $3$ | $11.81 \pm 0.12$ | $3.7 \pm 2.7$ | |
| Al II .............. | $3$ | $10.80 \pm 0.15$ | $4.0 \pm 3.2$ | |
| C II .............. | $1$ | $12.78 \pm 0.04$ | $5.6 \pm 0.9$ | |
| Si III .............. | $-31$ | $12.62 \pm 0.09$ | $19.9 \pm 5.8$ | |
| | $2$ | $12.87 \pm 0.09$ | $7.9 \pm 1.3$ | |
| Si IV ............. | $-32$ | $12.73 \pm 0.02$ | $20.1 \pm 1.4$ | |
| | $2$ | $13.28 \pm 0.01$ | $5.4 \pm 0.1$ | |
| C IV.............. | $-47$ | $13.25 \pm 0.16$ | $10.0 \pm 1.4$ | |
| | $-31$ | $13.24 \pm 0.41$ | $10.6 \pm 3.5$ | |
| | $-12$ | $13.40 \pm 0.28$ | $23.6 \pm 11.8$ | |
| | $3$ | $14.04 \pm 0.02$ | $6.1 \pm 0.2$ | |
| | $(-47)^{c}$ | $(13.27 \pm 0.03)^{c}$ | $(10.5 \pm 0.3)^{c}$ | x |
| | $(-28)^{c}$ | $(13.48 \pm 0.02)^{c}$ | $(13.8 \pm 0.5)^{c}$ | x |
| | $(5)^{c}$ | $(13.85 \pm 0.01)^{c}$ | $(5.3 \pm 0.1)^{c}$ | x |
| $z = 1.75570$ (HE 2243$-$6031) | | | | |
| H I ................ | $-1$ | $>14.85^{b}$ | $18.6 \pm 1.4$ | |
| Mg II............. | $0$ | $12.64 \pm 0.01$ | $5.4 \pm 0.1$ | x |
| Al III ............ | $2$ | $11.89 \pm 0.06$ | $4.7 \pm 1.3$ | |
| Si III .............. | $0$ | $13.08 \pm 0.07$ | $9.8 \pm 0.8$ | |
| Si IV ............. | $1$ | $13.65 \pm 0.01$ | $6.8 \pm 0.1$ | |
| C IV.............. | $-1$ | $14.72 \pm 0.06$ | $9.9 \pm 0.3$ | |
| | $(-1)^{c}$ | $(14.73 \pm 0.06)^{c}$ | $(9.8 \pm 0.3)^{c}$ | x |

[a] Measured column density of cloud is used to optimize on this transition in our photoionization model.
[b] Column densities of H I components measured from the best model are listed in col. (9) of Table 6.
[c] Voigt profile fit after removing contributions to this ion from the other phases.

model spectrum deviate greatly from the observed spectrum. It is not practical to apply formal procedures to assess the quality of fit because of the effect of blends and data defects on a $\chi^2$ statistic. If all transitions of a certain element are over/underproduced compared to the observed spectrum in the best model, we consider a specific abundance pattern for the system. Our method is illustrated for a specific example, the $v = 1$ km s$^{-1}$ cloud for the $z = 1.78169$ system toward HE 0141$-$3932 (system 1) in Figure 4. We show, for this component, that only values within the range $-0.7 < \log Z < 0.1$ and within 0.1 dex of $\log U = -2.3$
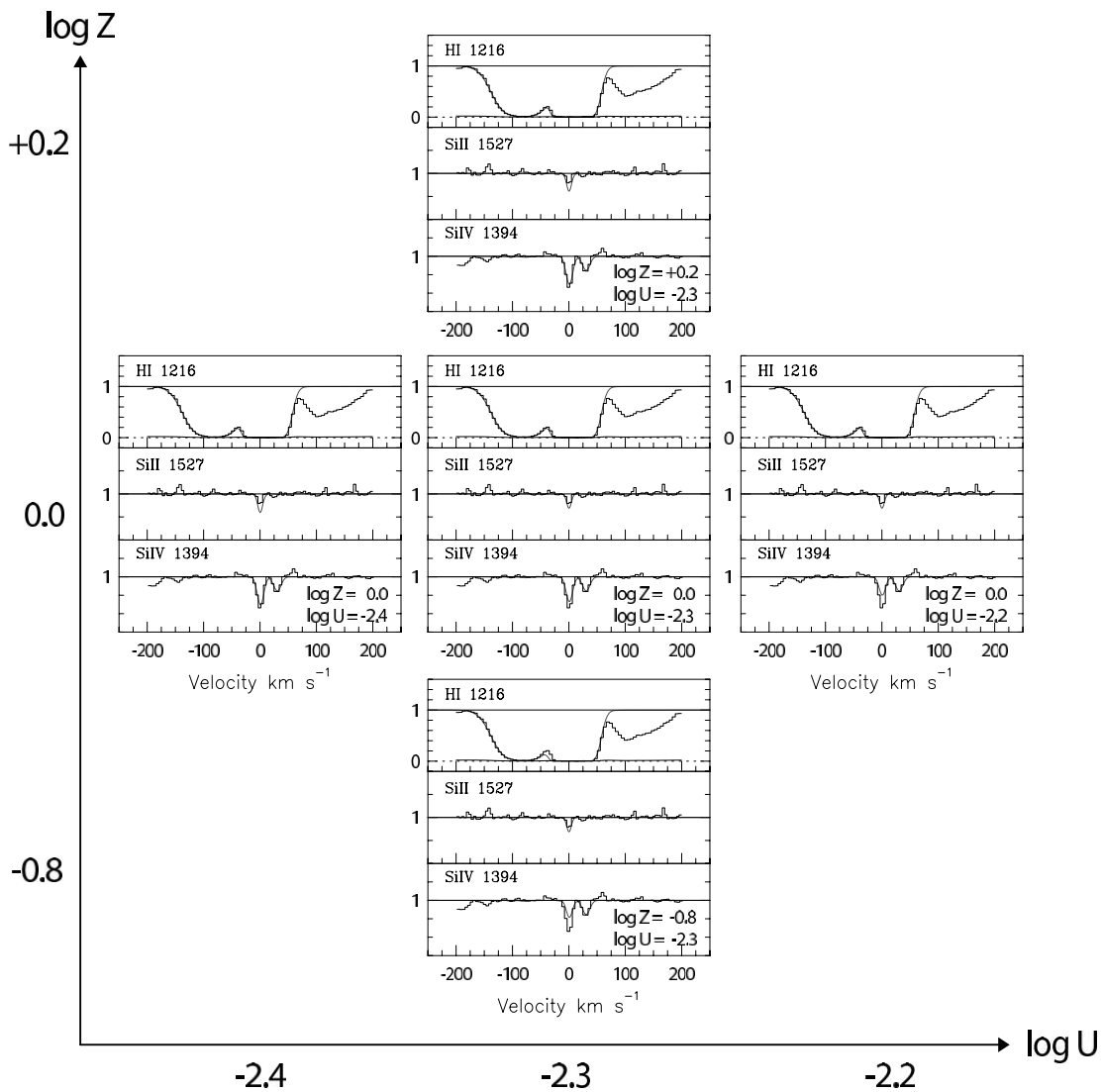
FIG. 4.—Synthetic model profiles from Cloudy models superimposed on the data for five sets of values of the ionization parameter ( log $U$ ) and metallicity ( log $Z$ ). The example plotted is the $v = 1$ km s$^{-1}$ cloud of the $z = 1.78169$ system toward HE 0141−3932. For other adjacent clouds the model parameters set at their preferred values and were not adjusted. The three transitions displayed were those that provided the strongest constraints on the parameters for this cloud. The normalized flux scale for the H I panel extends from 0 to 1, but the flux scales for the Si II and Si IV are expanded vertically to better show deviations between the models and the data. [*See the electronic edition of the Journal for a color version of this figure.*]

produce acceptable fits to Lyα, Si II, and Si IV, which are the main constraints for this case.

Usually, low-ionization phase clouds that produce the Mg II absorption lines also produce other low-ionization transitions such as Fe II, Si II, C II, and Al II. However, the higher-ionization transition, C IV, and sometimes intermediate-ionization transitions such as Si IV are not fully produced by the Mg II clouds. Therefore, once we find the best model for the Mg II clouds, we repeat a similar Cloudy analysis for the C IV clouds. For the high-ionization phase, multiple components are sometimes required to fit C IV absorption lines detected at different velocities. The results of Voigt profile fits to these C IV components are also listed in Table 3. Finally, the combined models, with contributions from both low- and high-ionization phases, are compared to the observed spectrum. Since Lyα absorption lines have contributions from both the low- and high-ionization phases, determination of metallicities for the low- and high-ionization phases can be degenerate. However, in the three single-cloud weak Mg II absorbers that we

are considering, it is possible to place limits on metallicity of both phases, so as not to overproduce the Lyα absorption. Also, in some cases, models with high metallicity ( leading to low temperatures) can be favored when comparing model profiles to some observed low-ionization transitions.

## 4. INDIVIDUAL SYSTEMS

For photoionization models, our procedure is adjusted for each system based on the available constraints in various transitions. Some transitions are blended with other lines, and others may be saturated. These issues are considered carefully during photoionization modeling. In this section we present the spectra of our three weak Mg II systems and then describe the results of photoionization models. We can place strong constraints on metallicity and ionization parameter because multiple transitions (including Lyα) have been detected in high S/N regions of the spectra (see Figs. 1–3). Hereafter we refer to the three weak Mg II systems as systems 1, 2, and 3. After presenting the constraints, we discuss

in § 4.4 the effect of varying model parameters and assumptions such as photoionization equilibrium, the shape of the incident radiation field, and the abundance of dust.

### 4.1. System 1 (HE 0141−3932; z = 1.78169)

This system is detected in Lyα, Mg II, Si II, Al II, C II, Al III, Si III, Si IV, and C IV, as shown in Figure 1. The observed spectrum covers Mg I, O I, and N V, but these transitions are not detected to a 5 σ detection limit. Although Fe II λ2383 is formally detected at only 3 σ and may be contaminated by spurious features, Fe II λ2600 is also detected at 2.5 σ, and both are precisely aligned with the Mg II. We therefore are confident in applying the Fe II as a constraint. Rest-frame equivalent widths and 5 σ equivalent width limits are listed in Table 2. Although the Lyα profile is complex, it provides a very strong constraint on metallicity because the flux at the position of the component centered on Mg II begins to recover on its blue side, which enables us to fit this component of Lyα effectively. All transitions except for high-ionization lines such as C IV and Si IV have only single components detected.

We begin by fitting a Voigt profile to the Mg II doublet. The best-fit parameters are listed in Table 3. A lower limit to the ionization parameter is provided by Fe II, which is overproduced at $\log U < -3.8$. Mg I is also overproduced at $\log U < -6.0$. (Mg I was not detected in the observed spectrum, and Fe II is only detected in the λ2383 transition at a level of ∼3 σ.) There is also a strict upper limit on the ionization parameter of $\log U < -2.8$, above which the high-ionization transitions C IV and Si IV are overproduced. Based on these considerations, models with $\log U = -3.8$ to $-2.8$ seem acceptable, although Si II and Al II provide additional constraints. An ionization parameter, $-3.8 < \log U < -3.7$, is consistent with all constraints. At lower values of $\log U$, Fe II is overproduced, and at higher values Al II and Si II are overproduced. Independent of the ionization parameter, the metallicity must be $\log Z > -0.7$ in order that Lyα is not overproduced. An upper limit of $\log Z < -0.5$ would also apply, for a solar abundance pattern, if $\log U = -3.7$, in order that Fe II absorption is not overproduced. The lower limit on metallicity of $\log Z > -0.7$ applies for the solar abundance pattern, and would be adjusted downward for an α-enhanced pattern. Similarly, $\log U$ could be lower in the α-enhanced case. If dust depletion were important, the lower limit on metallicity would be increased.

In addition to the Mg II cloud, three more higher ionization clouds are needed to reproduce the three detected C IV components, the two Si IV components, and the right wing of the Lyα profile. There are no N V lines detected, which is useful to place an upper limit on the ionization parameter. The results of Voigt profile fits to the C IV doublet are given in Table 3. Beginning with these C IV fits, we adjust the ionization parameter and metallicity to satisfy constraints from other transitions. In order to avoid overproduction of Si IV and low-ionization transitions (at low values) or N V (at high values), the ionization parameters for the additional three clouds at $\Delta v = -77$, 1, and 31 km s$^{-1}$ from the system center should be $-1.5 < \log U < -1.0$, $-2.35 < \log U < -2.25$, and $-1.9 < \log U < -1.8$, respectively. For these ionization parameters, lower limits on metallicity of $\log Z > -1.8$, $\log Z > -0.7$, and $\log Z > -0.5$ will apply for the three C IV components in order that Lyα is not overproduced. For the first two components, at $\Delta v = -77$ and 1 km s$^{-1}$ upper limits on $\log Z$ of 0.5 and 0.1 apply in order that low-ionization transitions are not overproduced. The third C IV component, at $\Delta v = 31$ km s$^{-1}$, has a strong constraint on its metallicity, assuming that

it is responsible for the Lyα absorption in the red wing of the profile (since the Mg II cloud cannot account for that absorption without overproducing Lyα in the blue wing). For that C IV we find that $-0.5 \lesssim \log Z \lesssim -0.4$ in order to match the Lyα profile. We emphasize that the three components have different ionization parameters from each other, although these values are all higher than that of the Mg II cloud.

The one Mg II and three C IV clouds reproduced all transitions except for Lyα. There are absorption features at both sides of the Lyα profile, at $\Delta v < -50$ and at $\Delta v > 70$ km s$^{-1}$ (see Fig. 1). Neither of them are Lyβ profiles from higher redshift systems, because the corresponding Lyα absorption lines would be located redward of the quasar Lyα emission line. The C IV component at $\Delta v = -77$ km s$^{-1}$ cannot itself give rise to all of the observed Lyα around that velocity because it is too narrow. Thus, we fit the broad Lyα profile [$b(\text{H}) = 42$ km s$^{-1}$ as listed in Table 3] and placed upper limits on its metallicity ( $\log Z < 0.0$ for $\log U \sim -3$ and $\log Z < -2.0$ for $\log U \sim -1.5$), so as not to produce other transitions at this velocity. The ionization parameter is not constrained for this broad Lyα cloud, although high values of $\log U$ are ruled out unless the metallicity is extremely small.

We conclude that for a solar abundance pattern, the metallicity of the $z = 1.78169$ weak Mg II system in the HE 0141−3932 spectrum is constrained to be $-0.7 \lesssim \log Z \lesssim -0.5$. A strict lower limit on metallicity of $\log Z > -0.7$ applies in order that Lyα absorption is not overproduced. Two of the three C IV clouds related to this system are constrained to have similar or higher metallicities, and for the other no significant metallicity constraint is available. The Mg II cloud has a subparsec size, much smaller than the three C IV phase absorbers, with sizes >10 pc. All components are optically thin, the Mg II cloud giving rise to $\log N_{\text{H I}} \sim 15.9$.

A summary of how specific transitions were used to constrain $\log U$ and $\log Z$ for this system is given in Table 4. Ranges of acceptable model parameters for each model cloud are listed in Table 5, in which column (1) is the absorption redshift, column (2) is the optimizing transition used in Cloudy, column (3) is the velocity shift from the system center, and column (4) is the acceptable range of ionization parameter. Column (5) of the table presents the best constraint on metallicity, considering both comparison to the observed Lyα and the fit to metal-line transitions, assuming a solar abundance pattern. Column (6) is a more conservative constraint on the metallicity of the cloud, using only the requirement that Lyα absorption is not overproduced. Column (7) is the depth of absorber along the line of sight, column (8) is the Doppler parameter of the optimizing transition (listed in col. [2]), and column (9) is the column density of neutral hydrogen gas in the absorbers. An example of a best-fit model and its specific parameters is presented in Figure 1 and Table 6.

### 4.2. System 2 (HE 0429−4091; z = 1.68079)

This is a very weak Mg II system whose rest-frame equivalent width [$W_r(2796) = 0.015$ Å] is just above the lower limit of the survey presented in Narayanan et al. (2007). In this system, Lyα, Si II, Al II, C II, Al III, Si III, Si IV, and C IV are clearly detected, but O I, Fe II, and N V are not detected at 5 σ, as shown in Figure 2. The rest-frame equivalent widths and 5 σ limits are tabulated in Table 2.

Again, we begin by fitting Voigt profiles to the Mg II doublet (see Table 3). Low ionization parameters, smaller than $\log U = -3.5$, are not acceptable because of overproduction of Fe II. At $\log U > -2.0$, C IV is overproduced. For this system, the Lyα absorption is strong, and it probably arises from offset C IV

TABLE 4
MODEL CONSTRAINTS FOR THREE WEAK Mg II SYSTEMS

| Cloud (1) | Parameter (2) | Constraint (3) | Line (4) | Condition (5) |
|---|---|---|---|---|
| System 1 | | | | |
| Mg II (0 km s$^{-1}$)........................ | log $U$ | >−3.8 | Fe II | To avoid overproduction |
| | | <−3.7 | Al II and Si II | To avoid overproduction |
| | | (>−6.0 | Mg I | To avoid overproduction) |
| | | (<−2.8 | C IV and Si IV | To avoid overproduction) |
| | log $Z$ | >−0.7 | Lyα | To avoid overproduction |
| | | <−0.5 | Fe II | To avoid overproduction at log $U$ ∼ −3.7 |
| C IV (−77 km s$^{-1}$)...................... | log $U$ | >−1.5 | Si IV and LI[a] | To avoid overproduction |
| | | <−1.0 | N V | To avoid overproduction |
| | log $Z$ | >−1.8 | Lyα | To avoid overproduction |
| | | <0.5 | LI[a] | To avoid overproduction |
| C IV (1 km s$^{-1}$)........................ | log $U$ | >−2.35 | Si IV and LI[a] | To avoid overproduction |
| | | <−2.25 | N V | To avoid overproduction |
| | log $Z$ | >−0.7 | Lyα | To avoid overproduction |
| | | <0.1 | LI[a] | To avoid overproduction |
| C IV (31 km s$^{-1}$)........................ | log $U$ | >−1.9 | Si IV and LI[a] | To avoid overproduction |
| | | <−1.8 | N V | To avoid overproduction |
| | log $Z$ | −0.5 to −0.4 | Lyα | To match the observed profile |
| | | (>−0.6 | Lyα | To avoid overproduction) |
| Lyα (−82 km s$^{-1}$)...................... | log $Z$ | <0.0 | | To produce no other transitions if log $U$ ∼ −3.0 |
| | | <−2.0 | | To produce no other transitions if log $U$ ∼ −1.5 |
| System 2 | | | | |
| Mg II (0 km s$^{-1}$)........................ | log $U$ | ∼−2.0 | C IV and Si IV | To match the observed profiles |
| | | (>−3.5 | Fe II | To avoid overproduction) |
| | | (<−2.0 | C IV | To avoid overproduction) |
| | log $Z$ | >−0.2 | Al II | To avoid overproduction |
| | | <0.1 | C IV and Si IV | To avoid underproduction |
| | | (>−3.0 | Lyα | To avoid overabsorption of the blue wing) |
| C IV (−47 km s$^{-1}$)...................... | log $U$ | −1.7 to −1.6 | Si III and Si IV | To match the observed profile |
| | log $Z$ | −1.1 to −1.0 | Lyα | To account for the blueward edge of Lyα profile |
| C IV (−28 km s$^{-1}$)...................... | log $U$ | ∼−1.8 | Si III and Si IV | To match the observed profile |
| | log $Z$ | >−1.8 | Lyα | To avoid overproduction |
| C IV (5 km s$^{-1}$)........................ | log $U$ | ∼−1.8 | Si III and Si IV | To match the observed profile |
| | log $Z$ | >−2.9 | Lyα | To avoid overproduction |
| | | <−0.3 | LI[a] | To avoid overproduction |
| Lyα (64 km s$^{-1}$)........................ | log $Z$ | <−2.0 | C IV and N V | To avoid overproduction if log $U$ > −2.0 |
| | | <0.0 | LI[a] | To avoid overproduction if log $U$ < −2.5 |
| System 3 (Model 1) | | | | |
| Mg II (0 km s$^{-1}$)........................ | log $U$ | ∼−2.0 | Al II, Al III, Si II | To match the observed profile |
| | | (>−3.5 | Fe II | To avoid overproduction) |
| | | (<−2.0 | Si IV | To avoid overproduction) |
| | | (<−1.5 | C IV | To avoid overproduction) |
| | log $Z$ | >0.9 | Al III | To avoid overproduction |
| | | (>0.4 | Si IV | To avoid overproduction) |
| | | (>0.0 | Lyα | To avoid overproduction) |
| C IV (0 km s$^{-1}$)........................ | log $U$ | −1.5 to −1.4 | Si IV | To match the observed profile |
| | log $Z$ | −0.1 to 0.0 | Lyα | To match the observed profile |
| System 3 (Model 2) | | | | |
| Mg II (0 km s$^{-1}$)........................ | log $U$ | ∼−2.0 | Al II, Al III, Si II | To minimize overproduction[b] |
| | | (>−3.5 | Fe II | To avoid overproduction) |
| | | (<−2.0 | Si IV | To avoid overproduction) |
| | | (<−1.5 | C IV | To avoid overproduction) |
| | log $Z$ | >0.0 | Lyα | To avoid overproduction[c] |
| C IV (0 km s$^{-1}$)........................ | log $U$ | ∼−1.1 | Si IV | To match the observed profile |
| | log $Z$ | >−0.2 | Lyα | To avoid overproduction |

[a] Low- and intermediate-ionization transitions including Mg I, Mg II, O I, C II, Fe II, Si II, Si III, Al II, and Al III.
[b] To match these profiles a reduction of the aluminum abundance by 0.5 and the silicon abundance by 0.2 can be applied.
[c] A log $Z$ > 0.0 is not required by Al II, Al III, and Si II if an abundance pattern adjustment is used.

TABLE 5
ACCEPTABLE MODELS FOR THREE WEAK Mg II SYSTEMS

| $z_{abs}$ (1) | Ion (2) | $\Delta v$ (km s$^{-1}$) (3) | $\log U$ (4) | $\log (Z/Z_\odot)$ (5) | $\log (Z/Z_\odot)_{min}$ (6) | Size (kpc) (7) | $b$ (km s$^{-1}$) (8) | $\log N$(H I) (cm$^{-2}$) (9) |
|---|---|---|---|---|---|---|---|---|
| 1.78169............ | Mg II | 0 | $-3.8$ to $-3.7$ | $-0.7$ to $-0.5$ | $>-0.8$ | 0.00051–0.0012 | 4 | 15.81–15.96 |
| | C IV | $-77$ | $-1.5$ to $-1.0$ | $-1.8$ to 0.5 | $>-1.9$ | 0.0072–13. | 9 | 12.58–13.42 |
| | C IV | 1 | $\sim-2.3$ | $-0.7$ to 0.1 | $>-0.8$ | 0.016–0.083 | 7 | 14.46–14.57 |
| | C IV | 31 | $-1.9$ to $-1.8$ | $-0.5$ to $-0.4$ | $>-0.6$ | 0.11–0.15 | 9 | 14.11–14.45 |
| | Ly$\alpha$ | $-82$ | ... | $<0.0$ | $<0.0$ | ... | 42 | ... |
| 1.68079............ | Mg II | 0 | $\sim-2.0$ | $-0.2$ to 0.1 | $>-3.0$ | 0.085–0.23 | 7 | 14.51–14.83 |
| | C IV | $-47$ | $-1.7$ to $-1.6$ | $-1.1$ to $-1.0$ | $>-1.1$ | 0.78–1.2 | 11 | 14.46–14.68 |
| | C IV | $-28$ | $\sim-1.8$ | $>-1.8$ | $>-1.8$ | $<11.$ | 14 | $<15.83$ |
| | C IV | 5 | $\sim-1.8$ | $-2.9$ to $-0.3$ | $>-3.0$ | 0.54–360 | 5 | 14.76–17.36 |
| | Ly$\alpha$ | 64 | ... | $<0.0$ | $<0.0$ | ... | 34 | ... |
| 1.75570 (model 1) ..... | Mg II | 0 | $\sim-2.0$ | $>0.9$ | $>0.0$ | $<0.019$ | 5 | $<14.70$ |
| | C IV | 0 | $-1.5$ to $-1.4$ | $-0.1$ to 0.0 | $>-0.2$ | 3.1–5.0 | 10 | 14.94–15.00 |
| 1.75570 (model 2) ..... | Mg II | 0 | $\sim-2.0$ | $\sim0.0$ | $>0.0$ | $\sim1.5$ | 5 | $\sim15.72$ |
| | C IV | 0 | $\sim-1.1$ | $>-0.2$ | $>-0.2$ | $<17.$ | 10 | $<14.81$ |

components rather than from the Mg II cloud. Because of the strong Ly$\alpha$ absorption we cannot place a meaningful constraint on the metallicity of the system; the blue wing of Ly$\alpha$ only requires $\log Z > -3.0$. However, at $-3.5 < \log U < -2.0$, Al II is overproduced at low metallicity (such that $\log Z > -1.0$ for $\log U \sim -3.0$ and $\log Z > -0.3$ for $\log U \sim -2.0$). Because the acceptable range of ionization parameters is large for this system, we consider two extreme cases: (1) the Mg II cloud has the highest acceptable ionization parameter ($\log U = -2.0$) that produces the maximum possible C IV and Si IV absorption; and (2) the Mg II cloud has the lowest acceptable ionization parameter ($\log U = -3.5$), so that it does not significantly contribute to the C IV and Si IV profiles. We refer to these below as the maximal and minimal C IV models.

In the maximal C IV model, we need an additional three high-ionization components to fit C IV profile at $\Delta v = -47, -28$, and 5 km s$^{-1}$ from the system center. The fitting parameters, after removing the contributions to C IV from the low-ionization clouds, are listed in Table 3. Figure 2 also shows that the Mg II cloud at 0 km s$^{-1}$ is offset and is not broad enough to explain all of the C IV absorption at a similar velocity. Only the C IV cloud at $\Delta v = -47$ km s$^{-1}$ has its metallicity constrained to be $\log Z = -1.1$ to $-1.0$, assuming that it accounts for the blueward edge of the saturated Ly$\alpha$ profile. The metallicity cannot be lower than this value or Ly$\alpha$ would be overproduced. However, a constraint on the ionization parameters of the three C IV clouds can be obtained by the requirement that they also fit the Si III and Si IV doublet profile. For the three C IV clouds, we find $\log U$ in the range between $-1.8$ and $-1.6$. The only disagreement between this maximal C IV model and the observed spectrum is an overproduction of N V. Adjusting the abundance pattern so that nitrogen is reduced by at least 0.5 dex compared to the other elements gives adequate results (see Fig. 2). In fact, the production mechanisms for nitrogen are poorly understood (e.g., Russel & Dopita 1992 and references therein). In specific, it is not well understood yet whether massive stars or intermediate-mass stars (or both) contribute to the *primary* nitrogen production before the *secondary* production starts through the CNO cycle (Spite et al. 2005). This nitrogen "problem" has also been reported frequently in DLA systems (e.g., Pettini et al. 2002) and for the Magellanic Bridge (e.g., Lehner et al. 2001), as well as for multiple-cloud weak Mg II systems (Zonak et al. 2004). Once the best model parameters for

the three C IV components are found, we adjust the parameters for Mg II again to compensate and get $\log U = -2.0$ and $\log Z = -0.2$ to 0.1. The lower limit on metallicity was placed in order not to overproduce Al II, and the upper limit in order not to underproduce Si IV and C IV. Acceptable ranges of model parameters for one Mg II and three C IV components (the maximal C IV model) are summarized in Table 5. An example of the best-fit model is overplotted on the observed spectrum in Figure 2. Here we emphasize that the Mg II component has a relatively high ionization parameter similar to those of the C IV components.

We also consider a minimal C IV model, for which we need four more components to reproduce C IV and Si IV because there is no contribution to the C IV absorption from the Mg II phase. We fit the C IV profile with four high-ionization phase clouds at $\Delta v$ of $-47, -31, -12$, and 3 km s$^{-1}$ from the system center. As with the maximal C IV model, the metallicity of the $\Delta v = -47$ km s$^{-1}$ component is constrained to be $\log Z = -1.0$ to $-0.9$. We found a range of acceptable ionization parameters for the first three C IV components, with $\log U = -1.9$ to $-1.7$. However, there are no acceptable solutions for the fourth component (that overlaps with the Mg II component). The best model, with $\log Z = -0.5$ and $\log U = -1.9$, reproduces observations for most all transitions, but it gives rise to additional Mg II absorption. These double contributions from low- and high-ionization phase clouds overproduce the observed Mg II profile. This result suggests that the Mg II absorption is partially produced by the same cloud as the C IV, and supports the maximal C IV model above. Thus, we conclude that the maximal C IV model with three C IV components is more appropriate to describe this system.

As with system 1, the right wing of the Ly$\alpha$ profile is not produced either by the Mg II cloud or by the three C IV clouds. Therefore, we placed an additional Ly$\alpha$ line in this region of the profile. The unexplained absorption cannot be Ly$\beta$ because this region is not in the Ly$\beta$ forest, as was the case with system 1. We fit the region using one additional Ly$\alpha$ component with $\log N_{H I} \sim 14.6$ and $b \sim 34$ km s$^{-1}$. This component is not well constrained, but for $\log U > -2.0$ C IV and N V are overproduced unless $\log Z < -2.0$. For $\log U < -2.5$, the metallicity can be as large as $\log Z = 0.0$ before low-ionization transitions are overproduced.

We conclude that the $z = 1.68079$ system in the HE 0429$-$4091 spectrum has three C IV components as well as one Mg II component. The transitions that provided constraints on $\log U$

TABLE 6
BEST-FIT MODELS FOR THREE WEAK Mg II SYSTEMS

| Cloud (1) | $v$ (km s$^{-1}$) (2) | log ($Z/Z_\odot$) (3) | log $U$ (4) | $n_H$ (cm$^{-3}$) (5) | Size (kpc) (6) | $T$ (K) (7) | log $N_{tot}$(H) (cm$^{-2}$) (8) | log $N$(H I) (cm$^{-2}$) (9) | log $N$(Mg II) (cm$^{-2}$) (10) | log $N$(Si IV) (cm$^{-2}$) (11) | log $N$(C IV) (cm$^{-2}$) (12) | $b$(H) (km s$^{-1}$) (13) | $b$(Mg) (km s$^{-1}$) (14) | $b$(C) (km s$^{-1}$) (15) | Abundance Pattern (16) |
|---|---|---|---|---|---|---|---|---|---|---|---|---|---|---|---|
| | | | | | | | $z = 1.78169$ (HE 0141−3932) | | | | | | | | |
| Mg II 1 ............. | 0 | −0.6 | −3.7 | 0.095 | 0.00096 | 11100 | 17.45 | 15.87 | 12.06 | 10.27 | 10.10 | 14 | 4 | 5 | Solar |
| C IV 1 ............... | −77 | −0.5 | −1.0 | 0.00019 | 0.43 | 24400 | 17.40 | 12.94 | 8.13 | 10.78 | 12.58 | 21 | 7 | 9 | Solar |
| C IV 2 ............... | 1 | 0.0 | −2.3 | 0.0038 | 0.019 | 8730 | 17.35 | 14.49 | 11.46 | 12.35 | 12.81 | 14 | 7 | 7 | Solar |
| C IV 3 ............... | 31 | −0.5 | −1.8 | 0.0012 | 0.15 | 17300 | 17.75 | 14.19 | 10.45 | 12.14 | 13.12 | 18 | 8 | 9 | Solar |
| Ly$\alpha$ 1 ............... | −82 | −1.0 | −2.5 | 0.0060 | 0.0094 | 17300 | 17.24 | 14.36 | 10.32 | 11.00 | 11.55 | 42 | 39 | 39 | Solar |
| | | | | | | | $z = 1.68079$ (HE 0429−4091) | | | | | | | | |
| Mg II 1 ............. | 0 | −0.1 | −2.0 | 0.0018 | 0.17 | 11200 | 17.98 | 14.74 | 11.53 | 12.94 | 13.63 | 15 | 7 | 7 | Solar |
| C IV 1 ............... | −47 | −1.0 | −1.6 | 0.00072 | 1.2 | 24500 | 18.43 | 14.55 | 10.12 | 12.02 | 13.26 | 22 | 10 | 11 | Solar |
| C IV 2 ............... | −28 | −1.0 | −1.8 | 0.0012 | 1.4 | 22600 | 18.70 | 15.04 | 10.78 | 12.45 | 13.49 | 23 | 13 | 14 | Solar |
| C IV 3 ............... | 5 | −1.0 | −1.8 | 0.0011 | 3.4 | 22500 | 19.08 | 15.42 | 11.16 | 12.83 | 13.86 | 18 | 4 | 5 | −0.5 dex (N) |
| Ly$\alpha$ 1 ............... | 64 | −1.0 | −2.5 | 0.0057 | 0.016 | 17300 | 17.45 | 14.57 | 10.53 | 11.20 | 11.75 | 34 | 30 | 30 | Solar |
| | | | | | | | $z = 1.75570$ (HE 2243−6031) | | | | | | | | |
| Model 1 | | | | | | | | | | | | | | | |
| Mg II 1 .......... | 0 | 1.0 | −2.0 | 0.0015 | 0.023 | 424 | 17.02 | 14.62 | 12.64 | 13.11 | 13.59 | 6 | 6 | 6 | Solar |
| C IV 1 ........... | 0 | −0.1 | −1.4 | 0.00047 | 5.0 | 15200 | 18.86 | 14.94 | 11.27 | 13.42 | 14.73 | 18 | 9 | 10 | Solar |
| Model 2 | | | | | | | | | | | | | | | |
| Mg II 1 .......... | 0 | 0.0 | −2.0 | 0.0018 | 1.5 | 9870 | 18.93 | 15.72 | 12.63 | 13.81 | 14.65 | 14 | 6 | 6 | −0.5 dex (Al), −0.2 dex (Si) |
| C IV 1 ........... | 0 | 0.2 | −1.1 | 0.00024 | 5.8 | 14700 | 18.63 | 14.43 | 10.61 | 13.14 | 14.72 | 18 | 10 | 10 | Solar |

and log $Z$ based on our Cloudy models are listed in Table 4. All components have similar ionization parameters, log $U \sim -1.9$. It is difficult to constrain the metallicity of the low-ionization phase for this system, since there are kinematically distributed C IV components that contribute to the Ly$\alpha$ absorption. However, metal line absorption is best reproduced with about solar metallicity for the Mg II component. The blueward, offset C IV cloud is constrained by the Ly$\alpha$ profile to have log $Z > -1.1$. Because of its higher ionization state, the size of the Mg II cloud of this system ($\sim$100 pc) is 2 orders of magnitude larger than that of the Mg II cloud in system 1. All components are optically thin. Ranges of acceptable model parameters are listed in Table 5. An example of the best models and its model parameters is presented in Figure 2 and Table 6. For the model curves shown in Figure 2, the nitrogen abundance is decreased by 0.5 dex from the solar abundance.

### 4.3. *System 3* (*HE 2243−6031; z = 1.75570*)

This weak Mg II system has simple, single-component profiles detected in Ly$\alpha$, the low-ionization lines, Mg II and Si II, and in the higher ionization lines, Al III, Si III, Si IV, and C IV. Fe II and Al II lines are not detected to a 5 $\sigma$ equivalent width limit. See Table 2 for the rest-frame equivalent widths and 5 $\sigma$ limit values. The regions of spectrum where O I, C II, and N V would appear are contaminated by blends, so that they only serve to provide weak upper limits. It is immediately apparent that the equivalent width of Mg II is very large for this system compared to its relatively weak Ly$\alpha$ profile. This implies that the system has a high metallicity. Velocity plots of various transitions are displayed in Figure 3.

As usual, we first optimize on the column density and Doppler parameter of Mg II obtained from Voigt profile fitting (see Table 3). A lower limit on the ionization parameter of log $U > -3.5$ can be determined, since Fe II is overproduced at smaller values. On the other hand, higher ionization conditions with log $U > -2.0$ are ruled out because of overproduction of Si IV. The observed C IV absorption is also overproduced if log $U > -1.5$.

More stringent constraints on the ionization parameter can be found if we consider the observed absorption in Al II and Si II. For metallicities log $Z \lesssim 0.0$, the constraints on ionization parameter are independent of metallicity. For larger metallicities, cooling leads to different constraints. We first consider the constraints for log $Z < 0.0$. Considering Al II and Si II, we found that an ionization parameter at the higher end of the range $-3.5 < $ log $U < -2.0$ produces the best agreement, but these ions are still overproduced by the model. To reconcile a log $U = -2.0$ model with the data for log $Z < 0.0$, we can reduce the abundance of aluminum by 0.5 dex and that of silicon by 0.2 dex. Further variations in abundance pattern could lead to different preferred values of log $U$.

Independent of the constraint on the ionization parameter, the Ly$\alpha$ profile can be used to place a strong lower limit on the metallicity of the Mg II cloud. The Mg II component is centered exactly on the Ly$\alpha$ profile, so that both the blue and the red side of the Ly$\alpha$ profile provide the same lower limit, log $Z > 0.0$, in order that Ly$\alpha$ is not overproduced. However, there are still some uncertainties on this metallicity constraint. On the one hand, lower values would be permitted if the system is in an $\alpha$-enhanced condition, because this constraint does assume a solar abundance pattern. On the other hand, the required metallicity would be higher if magnesium is depleted onto dust grains, although we do not expect a large amount of dust in weak Mg II systems, as discussed below. A cloud with log $U = -2.0$ and log $Z = 0.0$ has a temperature of $T = 9870$ K and a size of 1.5 kpc. A smaller

log $U$, which would be possible with further reductions in the abundances of aluminum and silicon, would lead to a smaller cloud size.

Metallicities greater than the solar value are also possible for the Mg II cloud. In fact, a solar abundance pattern can be consistent with the data because the cooling at high metallicity leads to less Al III and Si IV production. If we accept the constraint on ionization parameter of log $U \sim -2.0$, as discussed above, and assume a solar abundance pattern, we find that Si IV will be slightly overproduced unless log $Z > 0.4$. It is overproduced on the blue side of the Si IV $\lambda$1403 profile. For log $Z > 0.4$, Si IV is underproduced, but in this case Si IV absorption can arise from a second, higher ionization phase. Similarly, Al III is overproduced unless log $Z > 0.9$. (The $\lambda$1863 transition is overproduced; the $\lambda$1855 transition is contaminated by a blend.) Due to cooling at extreme metallicities, a log $Z = 1.0$ cloud would have a temperature of $\sim$500 K and a size of $\sim$25 pc. These constraints are quite dependent on abundance pattern. As we noted above, if the abundance of aluminum was decreased by 0.5 dex relative to the solar pattern and the silicon abundance was decreased by 0.2 dex, log $Z = 0.0$ would be consistent with the data for log $U = -2.0$. Both supersolar metallicity models and small changes in abundance patterns are reasonable ways to reconcile models with the data. However, we emphasize that the metallicity constraint of log $Z > 0.0$ is directly determined based on comparison with the Ly$\alpha$ profile.

Next we added a high-ionization phase because the broad-line profile of C IV cannot be reproduced by the low-ionization Mg II component (see the dotted line in Fig. 3 on the C IV profile). Si IV is also underproduced by an Mg II component with log $U = -2.0$ and log $Z = 1.0$. In order to find constraints on the C IV phase, we optimized on the C IV column density from our Voigt profile fit. In this case, the contribution to the C IV absorption from the low-ionization phase was minimal, so that removing it made no significant difference to the fit, listed in Table 3. From Cloudy photoionization models, we derive a constraint of log $U = -1.5$ to $-1.4$ on the ionization parameter, in order to simultaneously fit the C IV and Si IV profiles. If the metallicity of the Mg II cloud is lower, so that it gives rise to more Si IV absorption, then the ionization parameter of the C IV cloud would need to be higher to compensate. Similarly, if the ionization parameter of the Mg II cloud is lower, that of the C IV cloud would also need to be lower in order to produce more Si IV absorption.

Since the Ly$\alpha$ profile does not have a contribution from kinematically separate C IV components, it can be used to place a lower limit on the metallicity in the high-ionization phase. In order that Ly$\alpha$ is not overproduced by the C IV cloud, a metallicity of log $Z > -0.2$ is required. No firm upper limit can be placed, since the Ly$\alpha$ absorption would be fully accounted for by the Mg II cloud if log $Z = 0.0$. However, if the Mg II cloud has log $Z = 1.0$ in order to produce the observed Al III absorption, it does not account for all of the observed Ly$\alpha$ absorption. In this case, log $Z = -0.1$ to 0.0 for the C IV cloud would account for the majority of the Ly$\alpha$ absorption. A cloud with log $U = -1.4$ and log $Z = 0.0$ has a size of $\sim$5 kpc.

We conclude that the system can be reproduced with only two components: one low-ionization and one high-ionization phase. The constraints on log $U$ and log $Z$ and the transitions they were derived from are presented in Table 4 for two models. Model 1 assumes a solar abundance pattern and relies on a supersolar metallicity for the low-ionization phase to fit the data. Model 2 allows an adjustment of the abundances of aluminum and silicon relative to the solar pattern, but still requires at least a solar metallicity. Our favored two-phase model has a relatively high ionization

parameter of $\log U = -2.0$ for the Mg II cloud and $\log U = -1.4$ for the C IV cloud. However, with a different abundance pattern, the ionization parameter for the Mg II cloud could be lower. All components of acceptable models are optically thin in H I. Ranges of the acceptable model parameters are listed in Table 5, including both models with $\log Z = 0.0$ and with $\log Z > 0.9$ for the Mg II cloud. An example of best-fit models and their model parameters are presented in Figure 3 (only for the model with $\log Z > 0.9$) and Table 6 (for both).

### 4.4. *Effect of Photoionization Modeling Assumptions*

In using the Cloudy code to derive constraints for the three systems, we have assumed that photoionization equilibrium applies. This is almost certain to be the case for hydrogen since the photoionization timescale is short, on the order of $10^4$ yr. For metals, photoionization equilibrium might not apply if the gas has cooled from a higher temperature, in which case the gas would still be more ionized than our calculations would suggest. This would clearly affect our model constraints. However, our most important conclusion of high metallicities for weak Mg II absorber would only be stronger if a larger fraction of the magnesium was in higher ionization states.

Another important assumption we applied in our modeling was that of a solar abundance pattern, unless a deviation was required by the data. We note that deviations from the solar pattern are to be expected, and may apply whether the data require them or not. In other words, there is a degeneracy between the parameters $\log U$ and $\log Z$ and the abundance pattern. One common type of abundance pattern deviation would be an $\alpha$-enhanced condition. In this case, we tend to overestimate metallicity because our metallicity estimations are based on magnesium, an $\alpha$-element. Another source of the deviation is depletion onto dust grains. We do not really expect a large amount of dust in weak Mg II absorbers because they are not typically close to sites with large $N_{H I}$ or with current star formation. However, it is important to note that if magnesium is depleted by some factor, our inferred metallicity would *increase* by roughly that same factor.

Finally, we consider the effect of changing the shape of the ionizing radiation field. For the previous calculations we had assumed a Haardt and Madau model for the ionizing radiation from quasars and star-forming galaxies, with an escape fraction of 0.1 of ionizing photons from galaxies (Haardt & Madau 1996, 2001). We have also considered the opposite extreme, in which only quasars contribute to the ionizing radiation field. For a given ionization parameter, the absence of a stellar contribution leads to an increase in the relative number of high-energy photons. With that change of spectral shape, we found negligible difference in the properties derived for the low-ionization phase. For the high-ionization phase, we found that a lower ionization parameter (e.g., by about 0.5 dex) would be needed to fit the data. During the photoionization modeling presented above, we neglected possible contributions from nearby stellar sources. However, we see only small differences in the column densities of low/intermediate-ionization phase gas (e.g., Si II, Si III, and Si IV) by a factor of 2 or 3, even after adding stellar radiation from an O7 star with an effective temperature of $T_{\mathrm{eff}} = 38,000$ K (model C3 of Schaerer & de Koter 1997). We adopt an ionizing photon number density 10 times greater than that of the extragalactic background radiation, as a maximum flux model. Thus, contributions from nearby stellar sources, even if they exist, have no significant qualitative effect on our conclusions.

We conclude that none of the assumptions behind our photoionization models has a qualitative impact on our conclusions. In particular, there is no effect that works against our conclusion of a very high metallicity for system 3.

## 5. DISCUSSION

In this study we applied photoionization models to constrain the physical properties of three single-cloud weak Mg II absorption systems at $z \sim 1.7$. Along with results presented in Lynch & Charlton (2007), these complete a sample of the seven $z > 1.5$ single-cloud weak Mg II absorbers found in the VLT archive (Narayanan et al. 2007) for which metallicity constraints could be derived because of simultaneous coverage of various metal lines and Ly$\alpha$.

We start this final section by summarizing the model constraints derived for the three $z \sim 1.7$ single-cloud weak Mg II absorbers studied in this paper (§ 5.1). We then proceed to compare our results to the other four single-cloud weak Mg II systems at $z \sim 1.7$ from Lynch & Charlton (2007) in § 5.2. In this section we also compare to lower redshift single-cloud weak Mg II systems from the literature to investigate evolutionary trends. We address the high metallicity of these systems in the context of DLAs (whose metallicities are usually smaller than the solar value by a factor of 10–30) in § 5.3, of sub-DLAs in § 5.4, and of strong and multiple-cloud weak Mg II systems (the strong ones are usually associated with bright $[L > 0.05L^*]$ galaxies within 40 $h^{-1}$ kpc; e.g., Bergeron & Boissé 1991) in § 5.5. Finally, in § 5.6 we discuss a possible correlation between metallicity and total hydrogen column density.

### 5.1. *Summary of Results*

System 1 can be fit with a single low-ionization Mg II cloud and three higher ionization clouds (two of them offset in velocity from the Mg II) that give rise to C IV absorption. The low-ionization cloud has $\log Z > -0.8$ and two of the high-ionization clouds must have metallicities at least this high as well. Two offset low-metallicity clouds, producing only Ly$\alpha$ absorption, appear to be clustered with this system.

System 2 is also fit with one Mg II and three C IV clouds, although all four clouds have similar, relatively high ionization parameters ($\log U \sim -1.9$). The metallicity of the Mg II cannot be well constrained directly from comparison to the Ly$\alpha$ because the kinematical spread of the C IV lines give rise to a large Ly$\alpha$ equivalent width. However, near solar metallicities are possible, and even favored for a solar abundance pattern. Also, the blue-ward C IV cloud will overproduce absorption in Ly$\alpha$ unless its metallicity is $\log Z > -1.1$. A separate, offset low-metallicity component was again needed to fit the red portion of the Ly$\alpha$ profile.

System 3 has the best metallicity constraint among the seven single-cloud weak Mg II absorbers at $z > 1.5$ because of the absence of offset C IV components, thereby keeping the Ly$\alpha$ profile very narrow. Two phases are still required, with clouds of different ionization parameters centered at the same velocity that produce both the narrower low-ionization transitions and the broader high-ionization transitions. Both the low- and the high-ionization phases are constrained to have solar or supersolar metallicities.

The most striking thing about these model results is that in all three $z \sim 1.7$ systems, the metallicity of at least one phase of gas is constrained to be greater than 1/10 the solar value. The three systems all have at least two phases of gas: the low-ionization phase that arises in a layer of gas $\sim 1$–$100$ pc thick with a density of $0.001$–$0.1$ cm$^{-3}$, and the high-ionization phase that comes from a larger region ($\sim 0.1$–$10$ kpc) with a lower density. For these systems, even metallicities of the larger high-ionization phase
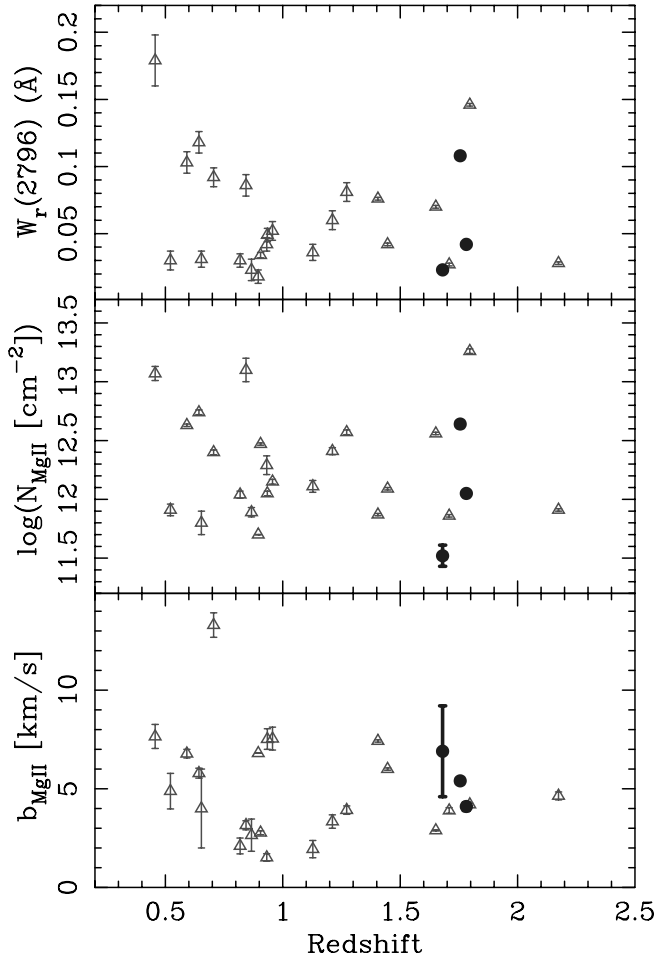
FIG. 5.—Rest-frame equivalent width [$W_r(2796)$; *top*], column density ($\log N_{Mg\,II}$; *middle*), and Doppler parameter ($b$; *bottom*) of weak Mg II systems plotted as a function of redshift between $z = 0.2$–2.5. Open triangles and error bars are taken from the literature (Rigby et al. 2002; Charlton et al. 2003; Ding et al. 2005; Lynch & Charlton 2007), while filled circles and error bars are from this paper. [*See the electronic edition of the Journal for a color version of this figure.*]

regions range from 1/10 solar up to solar. We return below to a discussion of the surprising issue of how regions with $\log N_{H\,I} <$ 15 (i.e., over a million times less than the threshold for star formation) can be enriched in metals to the solar value (§ 5.6).

### 5.2. *Comparison to Other Single-Cloud Weak* Mg II *Systems*

The properties of the three $z \sim 1.7$ single-cloud weak Mg II systems, derived from the observed profiles, are compared in Figure 5 to those of 23 other single-cloud weak Mg II absorbers, both at similar and at lower redshifts. Figure 5 shows that there is no significant evolution in the observed Mg II $\lambda2796$ profiles. Figure 6 presents quantities derived from photoionization models for our three absorbers and for others taken from the literature, using the same methods as we have used here (Rigby et al. 2002; Charlton et al. 2003; Ding et al. 2005; Lynch & Charlton 2007). The specific constraints that are displayed in Figures 5 and 6 are also listed in Table 7, with the relevant references.

Lynch & Charlton (2007) derived similar constraints for the phase structure of four different single-cloud weak Mg II absorbers at $z \sim 1.7$. They also placed constraints on the metallicities of those absorbers, of $\log Z > -1.5, > -1.5, > -1.0,$ and $> -2.0$ for the four different low-ionization phases. They note that the metallicities could be significantly higher than these lower limits,
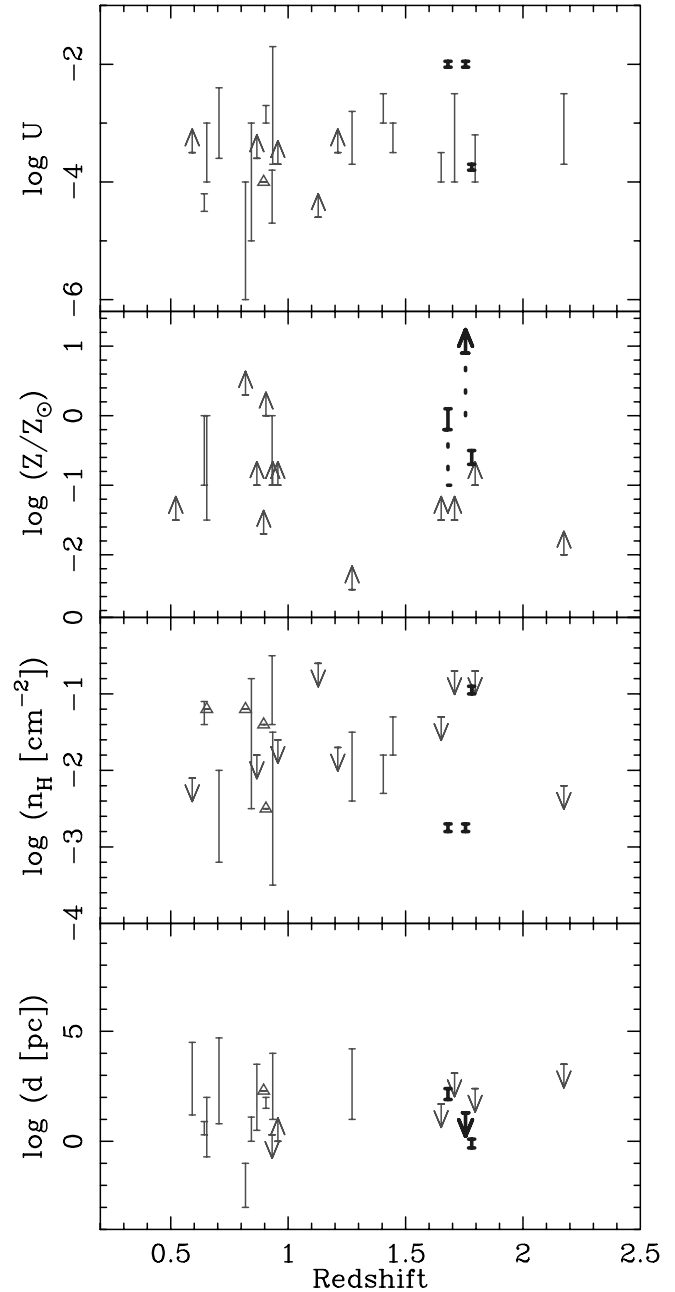


FIG. 6.—Same as Fig. 5, but for ionization parameter ($\log U$; *top*), metallicity ($\log Z$; *second from top*), hydrogen volume number density ($\log n_H$; *third from top*), and size of absorber ($\log d$; *bottom*). [*See the electronic edition of the Journal for a color version of this figure.*]

however, these absorbers (by chance) tended to have larger contributions to the Ly$\alpha$ absorption from offset C IV clouds and from Ly$\alpha$-only clouds.

Results from modeling lower redshift ($0.4 < z < 1.4$) single-cloud weak Mg II systems also typically yield a two-phase structure, with similar densities. Metallicity constraints are again often limited because of the difficulty in separating the contributions of the two phases. However, of the 11 cases of single-cloud weak Mg II absorbers for which some metallicity constraint could be obtained, two cases require the metallicity of the low-ionization phase to be solar or even supersolar (Charlton et al. 2003). Furthermore, a total of 7/11 of the low-redshift cases required a metallicity of at least 1/10 of the solar value. We note that the

## TABLE 7
### Single-Cloud Weak Mg II Systems from the Literature

| QSO | $z_{abs}$ | $\log N_{Mg\,II}$ (cm$^{-2}$) | $b_{Mg\,II}$ (km s$^{-1}$) | $\log U$ | $\log Z$ | $\log n_H$ (cm$^{-3}$) | $\log d$ (pc) | EW(2796) (Å) | $T_{gas}$ (K) | $\log N_{H\,I}$ (cm$^{-2}$) | $\log N_{tot}$ (cm$^{-2}$) | References |
|---|---|---|---|---|---|---|---|---|---|---|---|---|
| Q1421+331 .................. | 0.4564 | 13.07 ± 0.06 | 7.7 ± 0.6 | . . . | . . . | . . . | . . . | 0.179 ± 0.019 | . . . | . . . | . . . | 1 |
| Q1354+193 .................. | 0.5215 | 11.91 ± 0.05 | 4.9 ± 0.9 | . . . | >−1.5 | . . . | . . . | 0.030 ± 0.007 | . . . | . . . | . . . | 1 |
| Q0002+051 .................. | 0.5915 | 12.63 ± 0.01 | 6.8 ± 0.2 | >−3.5 | . . . | <−2.1 | 1.2−4.5 | 0.103 ± 0.008 | . . . | . . . | . . . | 1 |
| Q0454+036 .................. | 0.6428 | 12.74 ± 0.02 | 5.8 ± 0.3 | −4.5 to −4.2 | −1.0 to 0.0 | −1.4 to −1.1 | 0.3−0.9 | 0.118 ± 0.008 | . . . | . . . | . . . | 1 |
| PG 1634+706 ............... | 0.6534 | 11.80 ± 0.10 | 4.0 ± 2.0 | −4.0 to −3.0 | −1.5 to 0.0 | −1.2 to −1.2 | −0.7 to 2.0 | 0.031 ± 0.006 | 11,000 | 15.1−16.7 | 17.5 | 4 |
| Q0823−223 .................. | 0.7055 | 12.40 ± 0.02 | 13.3 ± 0.6 | −3.6 to −2.4 | . . . | −3.2 to −2.0 | 0.8−4.7 | 0.092 ± 0.007 | . . . | . . . | . . . | 1 |
| PG 1634+706 ............... | 0.8181 | 12.04 ± 0.03 | 2.1 ± 0.4 | −6.0 to −4.0 | >0.3 | −1.2 to −1.2 | −3.0 to −1.0 | 0.030 ± 0.005 | 4600 | 15.6−15.9 | 16.3 | 4 |
| Q1421+331 .................. | 0.8433 | 13.10 ± 0.10 | 3.2 ± 0.2 | −5.0 to −3.0 | . . . | −2.5 to −0.8 | 0−1.1 | 0.086 ± 0.008 | . . . | . . . | . . . | 1 |
| Q0002+051 .................. | 0.8665 | 11.89 ± 0.04 | 2.7 ± 0.8 | >−3.6 | >−1.0 | <−1.8 | 0.5−3.5 | 0.023 ± 0.008 | . . . | . . . | . . . | 1 |
| PG 1241+176 ............... | 0.8954 | 11.70 ± 0.00 | 6.8 ± 0.0 | −4.0 to −4.0 | >−1.7 | −1.4 to −1.4 | 2.3−2.3 | 0.018 ± 0.005 | 6500 | 15.2−15.2 | 16.3 | 2 |
| PG 1634+706 ............... | 0.9056 | 12.47 ± 0.01 | 2.8 ± 0.1 | −3.0 to −2.7 | >0.0 | −2.5 to −2.5 | 1.5−2.0 | 0.034 ± 0.002 | 9000 | 15.7−15.7 | 18.1 | 4 |
| Q0454+036 .................. | 0.9315 | 12.29 ± 0.08 | 1.5 ± 0.2 | −4.7 to −3.8 | −1.0−0.0 | −1.4 to −0.5 | <0.3 | 0.042 ± 0.005 | . . . | . . . | . . . | 1 |
| Q1206+456 .................. | 0.9343 | 12.05 ± 0.02 | 7.5 ± 0.5 | −3.7 to −1.7 | >−1.0 | −3.5 to −1.5 | 1−4.0 | 0.049 ± 0.005 | . . . | . . . | . . . | 1 |
| Q0002+051 .................. | 0.9560 | 12.15 ± 0.02 | 7.5 ± 0.6 | >−3.7 | >−1.0 | <−1.6 | >0 | 0.052 ± 0.007 | . . . | . . . | . . . | 1 |
| Q1213−003 .................. | 1.1278 | 12.11 ± 0.05 | 1.9 ± 0.4 | >−4.6 | . . . | <−0.6 | . . . | 0.036 ± 0.006 | . . . | . . . | . . . | 1 |
| Q0958+551 .................. | 1.2113 | 12.41 ± 0.03 | 3.3 ± 0.3 | >−3.5 | . . . | <−1.7 | . . . | 0.060 ± 0.007 | . . . | . . . | . . . | 1 |
| Q0958+551 .................. | 1.2724 | 12.57 ± 0.02 | 3.9 ± 0.2 | −3.7 to −2.8 | >−2.5 | −2.4 to −1.5 | 1−4.2 | 0.081 ± 0.007 | . . . | . . . | . . . | 1 |
| HE 2347−4342 ............. | 1.4054 | 11.87 ± 0.01 | 7.4 ± 0.1 | −3.0 to −2.5 | . . . | −2.3 to −1.8 | . . . | 0.076 ± 0.001 | . . . | . . . | . . . | 3 |
| Q0002−422 .................. | 1.4465 | 12.09 ± 0.01 | 6.0 ± 0.1 | −3.5 to −3.0 | . . . | −1.8 to −1.3 | . . . | 0.042 ± 0.001 | . . . | . . . | . . . | 3 |
| HE 0001−2340 ............. | 1.6515 | 12.56 ± 0.01 | 2.9 ± 0.0 | −4.0 to −3.5 | >−1.5 | <−1.3 | <1.7 | 0.070 ± 0.001 | . . . | . . . | . . . | 3 |
| HE 0429−4901 ............ | 1.6808 | 11.52 ± 0.09 | 6.9 ± 2.3 | −2.05 to −1.95 | −0.2−0.1 | −2.8 to −2.7 | 1.9−2.4 | 0.015 ± 0.001 | 11,200 | 14.5−14.8 | 18.0 | 5 |
| HE 0151−4326 ............ | 1.7085 | 11.86 ± 0.01 | 3.9 ± 0.1 | −4.0 to −2.5 | >−1.5 | <−0.7 | <3.1 | 0.027 ± 0.001 | . . . | . . . | . . . | 3 |
| HE 2243 −6031 ........... | 1.7557 | 12.64 ± 0.01 | 5.4 ± 0.1 | −2.05 to −1.95 | >0.9 | −2.8 to −2.7 | <1.3 | 0.121 ± 0.003 | 460 | <14.7 | 17.0 | 5 |
| HE 0141−3932 ............. | 1.7817 | 12.05 ± 0.01 | 4.1 ± 0.2 | −3.8 to −3.7 | −0.7 to −0.5 | −1.0 to −0.9 | −0.3−0.1 | 0.039 ± 0.001 | 11,100 | 15.8−16.0 | 17.5 | 5 |
| HE 2347−4342 ............ | 1.7962 | 13.26 ± 0.02 | 4.2 ± 0.1 | −4.0 to −3.2 | >−1.0 | <−0.7 | <2.4 | 0.146 ± 0.001 | . . . | . . . | . . . | 3 |
| HE 0940−1050 ............. | 2.1745 | 11.91 ± 0.01 | 4.6 ± 0.2 | −3.7 to −2.5 | >−2.0 | <−2.2 | <3.5 | 0.028 ± 0.001 | . . . | . . . | . . . | 3 |

REFERENCES.—(1) Rigby et al. 2002 and Churchill & Charlton 1999; (2) Ding et al. 2005; (3) Lynch & Charlton 2007; (4) Charlton et al. 2003; (5) this paper.

metallicities are often quite likely to be higher than these strict lower limits, because they are derived assuming that none of the Ly$\alpha$ absorption comes from the high-ionization clouds.

We conclude that some fraction of weak Mg II systems has been demonstrated to have solar or supersolar metallicity at low redshift (two systems at $z_{abs} = 0.8181$ and $0.9056$; Charlton et al. 2003) and even at $z \sim 1.7$ (one system at $z_{abs} = 1.7557$; this paper), which corresponds to an age of the universe of 3.7 Gyr. Values constrained to be greater than 1/10 the solar value are even more common. Furthermore, it is likely that in many cases for which lower limits on metallicity have been derived the actual value is much higher. The metallicity constraint that we have derived for the $z_{abs} = 1.7557$ absorber in this paper is high because this system is a rare case that does not have offset C IV absorption that contributes to the Ly$\alpha$ absorption. In other respects there is no reason to think it is unusual. The same applied for the low-redshift weak Mg II systems with the highest metallicity constraints (Charlton et al. 2003). We therefore know that single-cloud weak Mg II absorbers at both low and high redshift definitely have metallicities of at least 1/10 solar, but that some and probably many have solar or even supersolar metallicities.

Thus, even before $z = 1.5$, star formation must have polluted certain environments with metal-rich gas. Since Lynch & Charlton (2007) could not constrain any $z > 1.5$ single-cloud weak Mg II absorbers to have close to solar metallicity, and since several lower redshift solar metallicity cases were known, they tentatively suggested that there might be a gradual buildup of metals in the single-cloud weak Mg II absorber population. In this paper we have shown there is at least one strong counterexample, i.e., of $z > 1.5$ solar metallicity cases, and therefore there appears to be no metallicity evolution in the population. This is not to say that the population has a narrow range of physical properties: there is a large spread of cloud densities and metallicities at all redshifts (see Fig. 6). However, it does suggest that common processes are at work to create the metals and that the metals are mixed into fairly similar surrounding environments.

The existence of high-metallicity (greater than solar) compact intergalactic clouds ($\sim 100$ pc) has also been demonstrated by Schaye et al. (2007), who derived robust lower limits on metallicities of C IV absorbers using similar photoionization modeling techniques. Schaye et al. (2007) find that the number density of this population of high-metallicity C IV absorbers is of the same order as that of single-cloud weak Mg II absorbers and suggests that the former might evolve from the latter as material expands. More observations allowing direct connections between these populations will be of great interest. In fact, two of our three $z > 1.5$ weak Mg II systems have C IV phases with metallicities comparable to those derived by Schaye et al. (2007) for the high-metallicity C IV cloud population.

### 5.3. Comparison to Damped Ly$\alpha$ Systems

Damped Ly$\alpha$ systems, whose neutral hydrogen column densities are greater than $\log N_{H I} = 20.3$, dominate the neutral gas in the universe at high redshift (e.g., Lanzetta et al. 1995; Storrie-Lombardi & Wolfe 2000; Péroux et al. 2003). By identifying metal absorption lines that correspond to high-redshift DLAs, it is possible to constrain the global metal abundances and trace the evolution of metallicity in neutral gas from $z = 5$ to 0 (e.g., Pettini et al. 1994; Prochaska & Wolfe 2000).

However, the metallicity evolution measured from DLAs has two big problems: (1) the global mean metallicity is less than 1/6 of the solar abundance at $z > 1$ (e.g., Pettini et al. 1999; Prochaska & Wolfe 2000) and is still less than the solar by a factor of >4 if the metallicity-redshift relationship is extrapolated down

to $z \sim 0$ using a least-squares linear fit (Prochaska et al. 2003; Kulkarni et al. 2005; Péroux et al. 2006b);[6] and (2) the metallicity is also much smaller than the theoretically expected value from the star-forming activity at higher redshift (e.g., Madau et al. 1998; Pettini et al. 1999; Wolfe et al. 2003). This discrepancy (i.e., "missing-metals problem") remains an unresolved problem.

There are at least two possible classes of ideas proposed for the origin of this discrepancy: (1) a large amount of dust in metal-rich DLAs obscures background quasars, which prevent us from detecting DLAs with higher metallicities (e.g., Boisse et al. 1998; Fall & Pei 1993; Vladilo & Péroux 2005); and (2) the DLA region is sampling a lower metallicity than is found in the star-forming parts of the galaxy (Ellison et al. 2005b; Wolfe et al. 2003).

The dust obscuration scenario is supported by the small abundances of depleted elements such as Cr and Fe, relative to undepleted elements like Zn, in DLA systems (e.g., Pettini et al. 1997; Khare et al. 2004). Vladilo & Péroux (2005) estimated that $\sim 30\%-50\%$ of DLAs are missed as a consequence of obscuration. In absorbers expected to have a lower dust abundance, sub-DLA systems (super-LLSs) with $\log N_{H I} = 19.0-20.3$, a higher metallicity has been measured (e.g., Péroux et al. 2006a; Prochaska et al. 2006; Pettini et al. 2000; Kulkarni et al. 2007). Although Ellison et al. (2001) did not see any significant differences in DLAs toward radio-selected quasars, compared to those toward optically selected quasars at $z > 2$, the dust-depletion effect is expected to be more important at lower redshift.

Alternatively, Ellison et al. (2005b) and Chen et al. (2005) suggest that there could be a metallicity gradient as a function of a distance from the galactic center, with DLAs produced at a larger impact parameter than the stellar emission. DLAs that are produced in the host galaxies of gamma-ray bursts tend to have higher metallicities (e.g., Djorgovski et al. 2004), which could be more representative of typical star-forming regions. Also, small regions with DLA column densities could be ejected from galaxies by superwinds or as a part of AGN outflows (Mac Low & Ferrara 1999; Hamann et al. 1997; Gabel et al. 2006; Bouché et al. 2006).

Figure 7 summarizes the metallicities derived for DLAs at $z = 0.4-4.8$ from Prochaska et al. (2003) and Kulkarni et al. (2005), and compares to the values for single-cloud weak Mg II absorbers. It is striking that weak Mg II absorbers, despite having drastically smaller $N_{H I}$ values, have considerably higher metallicities than the DLAs, both at low redshift and at $z \sim 1.7$.

Because they are not near regions with current star formation, the dust-to-gas ratio in single-cloud weak Mg II absorbers is expected to be very small. Even for DLAs, it has been demonstrated that there is no bias against observing high metallicities due to the dust obscuration of their background quasars (Ellison et al. 2001, 2005a). Even if the dust-to-gas ratio is similar to those in DLAs, their total dust column density should be much smaller than those in DLAs, because of their lower gas column densities. Thus, they would not be subject to the metallicity bias that was more likely to have affected DLAs. Thus, the weak Mg II absorbers provide an opportunity to see some high-metallicity regions of the universe at high redshift, although they are not the same type of regions that would produce high-metallicity DLA absorption.

Relating to the idea that DLAs sample low-metallicity parts of galaxies, the weak Mg II absorbers, despite their low column densities, must somehow sample higher metallicity regions that are not closely related to luminous galaxies. This provides clear

---

[6] At $z < 1$, there are only a few cases of metallicity measurements in DLAs using high-quality spectra, and in these cases the metallicity is evaluated to be $\sim 1/10$ of the solar value (de la Varga et al. 2000; Pettini et al. 2000).
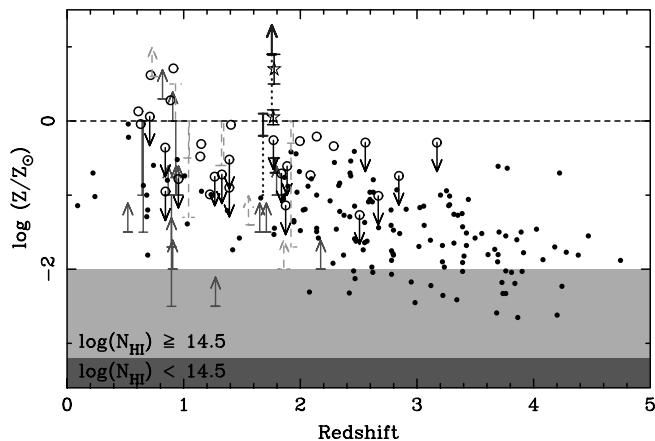
FIG. 7.—Metallicity in single-cloud weak Mg II systems as a function of redshift (*solid/dotted error bars*), compared to that of 148 DLA systems (*solid points*; Prochaska et al. 2003 and Kulkarni et al. 2005), 30 sub-DLA systems (*open circles*; Kulkarni et al. 2007), 10 Lyman limit systems including strong Mg II and multiple-cloud weak Mg II systems (*dashed error bars*; Lynch & Charlton 2007; Masiero et al. 2005; Zonak et al. 2004; Ding et al. 2003; Prochaska & Burles 1999), Ly$\alpha$ forest clouds with $\log N_{\rm H\,I} \geq 14.5$ (*thin shaded region*; Songaila & Cowie 1996; Cowie et al. 1995; Tytler et al. 1995), and Lyman $\alpha$ forest clouds with $\log N_{\rm H\,I} < 14.5$ (*thick shaded region*; Cowie & Songaila 1998; Lu et al. 1998). At $z \sim 1.7$, the three thick error bars with dotted lines are the more conservative metallicity constraints for the single-cloud weak Mg II systems that we have modeled (using Ly$\alpha$ as a direct constraint), and the two open stars are the supersolar sub-DLA systems from Prochaska et al. (2006). The horizontal dotted line denotes the solar metallicity. [*See the electronic edition of the Journal for a color version of this figure.*]

evidence for metallicity inhomogeneities, which because of the size constraints for single-cloud weak Mg II absorbers, are on very small scales (parsecs to hundreds of parsecs).

### 5.4. Comparison to sub-DLA Absorbers

Sub-DLA absorbers, with $\log N_{\rm H\,I} = 19.0$–20.3, have been found to have systematically higher metallicities than DLAs with the $N_{\rm H\,I}$-weighted value larger by 0.5–0.8 dex, at $0.6 < z < 3.2$ (Kulkarni et al. 2007). Several sub-DLA systems (super-LLSs) at $0.5 < z < 2.0$ have been found with metallicities that are solar or supersolar (e.g., Péroux et al. 2006a; Prochaska et al. 2006). Even small numbers of such high-metallicity systems contribute significantly to the total metal mass density at high redshift (Prochaska et al. 2006; Kulkarni et al. 2007). The Kulkarni et al. (2007) mean values of metallicity for sub-DLAs, determined from [Zn/H], are reproduced in our Figure 7 from their Table 1. Although there is a range of metallicities at each redshift, there is a clear increase in the metallicity of sub-DLAs from $\langle z \rangle = 1.5$ to 0.9. This is consistent with the global star formation history in the universe over this period, and the metallicity values are much more in line with expectations from chemical evolution models than those for DLAs (Kulkarni et al. 2007; Somerville et al. 2001).

Some single-cloud weak Mg II absorbers, with $\log N_{\rm H\,I} \sim 15$–16, also have solar or supersolar metallicities, both at $\langle z \rangle = 0.9$ and at 1.5. There is considerable overlap between the metallicity constraints for sub-DLAs and single-cloud weak Mg II absorbers at low and intermediate redshifts. However, it is important to note that many of the weak Mg II metallicities are only lower limits, and it is quite likely that the values are higher at least in some cases. The reason that we cannot derive higher metallicities for those systems could simply be the separate C IV clouds that happen to overlap in velocity. It is also important to note that for $z \sim 1.7$, the redshift of the absorbers we have studied in this paper, there are not many sub-DLA systems with supersolar met-

allicity, but all single-cloud weak Mg II absorbers potentially could have solar or supersolar metallicity, because we can place only lower limits on metallicity. Although two supersolar metallicity sub-DLAs were investigated by Prochaska et al. (2006), they were selected for study from a much larger sample because of their extremely strong Zn II absorption. However, much larger data samples of sub-DLAs and weak Mg II systems will be required before concluding whether there are any differences of metallicity between these two categories.

Another apparent difference between the metallicities of single-cloud weak Mg II absorbers and sub-DLAs, is that there is no clear increase in the metallicity of the single-cloud weak Mg II absorbers over the range $0.4 < z < 1.7$. This type of absorption is apparently produced by the same types of regions present over this redshift range, although they are known to be less common at low redshifts and at $z > 2$ (Narayanan et al. 2005, 2007; Lynch et al. 2006; Lynch & Charlton 2007).

The sample size of weak Mg II systems is now much smaller than those for DLAs and sub-DLAs, and only a few cases have been confirmed to have supersolar metallicities. It is quite important to increase the sample size of weak Mg II absorbers, particularly to include other systems with only one C IV component such that a strong constraint on metallicity can be derived. At $z < 1.5$ this will involve high-resolution observations with the *Hubble Space Telescope* COS or STIS of quasars for which high-resolution optical spectra are also available.

### 5.5. Comparison to Strong Mg II and Multiple-Cloud Weak Mg II Absorbers

Intermediate in $\log N_{\rm H\,I}$ between single-cloud weak Mg II absorption and sub-DLAs are Lyman limit and partial Lyman limit systems, with $\log N_{\rm H\,I} = 16$–19. These populations loosely correspond to the bulk of the strong Mg II absorber population, with $W_r(2796) > 0.3$ Å, and to multiple-cloud weak Mg II absorbers. Fewer of these systems have been studied in detail to date, but it is still possible to derive good constraints on metallicities in many cases, using photoionization modeling techniques the same as those employed here. The 10 cases of strong and multiple-cloud weak Mg II absorbers at $0.7 < z < 1.9$ (Masiero et al. 2005; Zonak et al. 2004; Lynch & Charlton 2007; Prochaska & Burles 1999; Ding et al. 2003), shown on Figure 7, have metallicities in the range $-1.5 < \log Z < 0.6$. These are consistent with the ranges for both sub-DLAs and single-cloud weak Mg II absorbers, but tend to be higher than those for DLAs. Without larger samples, we cannot distinguish differences or evolutionary trends, but again we note that many of these are measurements of the metallicity, while for the single-cloud weak Mg II absorbers the low metallicity values are all lower limits.

### 5.6. Metallicity versus $N_{\rm H\,I}$

In summary, Figure 7 shows that it is the lowest $N_{\rm H\,I}$ systems that appear to have the highest metallicities, both at $z < 1$ and at $z \sim 1.7$. The data are even consistent with a gradual increase in metallicity with decreasing $N_{\rm H\,I}$, although there is a huge spread at any given value. Such a trend has already been pointed out using compiled samples of DLAs and sub-DLAs (Boisse et al. 1998; Akerman et al. 2005; Meiring et al. 2006; Khare et al. 2007), extending down to sub-DLAs with $\log N_{\rm H\,I} \sim 19$ (Péroux et al. 2003). York et al. (2006) also suggested that a similar trend continued to strong Mg II systems with smaller hydrogen column densities.

The individual systems plotted on Figure 7, however, are only the systems with detected Mg II absorption. In particular, for single-cloud weak Mg II absorbers we are sure to be missing objects

with metallicities significantly less than those of the systems that we do detect. In fact, those lower metallicity objects are part of the much larger Ly$\alpha$ forest population. Figure 7 also shows the typical metallicities of Ly$\alpha$ forest clouds, both those with $\log N_{\rm H\,I} > 14.5$, which have $\log Z \lesssim -2.0$ (Songaila & Cowie 1996; Cowie et al. 1995; Tytler et al. 1995), and those with lower column densities, which have a mean metallicity of $\log Z \lesssim -3.2$ (Cowie & Songaila 1998; Lu et al. 1998). These much lower values for the Ly$\alpha$ forest overlap with the DLA metallicities at $z > 2.5$ but are smaller than those for low-redshift DLAs.

The fact that the high-metallicity population of single-cloud weak Mg II absorbers represents only a small fraction of all Ly$\alpha$ forest clouds does not diminish their significance. The single-cloud weak Mg II absorbers at $z \sim 1$ would account for 25%–100% of the Ly$\alpha$ forest clouds with $15.8 < \log N_{\rm H\,I} < 16.8$ (Rigby et al. 2002). More importantly, the cross-section of single-cloud weak Mg II absorbers in the plane of the sky is comparable to that of galaxies at $z \sim 1$, considering the regions of galaxies $\lesssim 30$–40 kpc that produce Lyman limit absorption. Thus, there are significant regions of the universe covered by these mysterious near-solar or supersolar metallicity objects with small $\log N_{\rm H\,I}$.

As described above, one explanation proposed for the larger metallicities for sub-DLAs than for DLAs is the dust obscuration of quasars that have the highest metallicity DLAs in their foregrounds. Although there may be some debate about whether this is a plausible explanation of that trend, it is not likely to explain the continued increase in metallicity toward the lowest $\log N_{\rm H\,I}$ weak Mg II absorbers. There is not likely to be a large selection effect due to dust obscuration for even the sub-DLA systems. It seems more plausible that different types of absorbers are sampling different types of regions in and around galaxies, which can have large variations in metallicities even on small scales. Different types of galaxies, e.g., star-forming versus quiescent, will have different fractions of area covered by regions of the different types. By comparing to the mass-metallicity relation seen in star-forming galaxies in the local universe (Tremonti et al. 2004) and at higher redshift (Savaglio et al. 2005; Erb et al. 2006), York et al. (2006) and Khare et al. (2007) proposed that the DLAs are associated with low-mass ($<10^9 \, M_\odot$) galaxies, while sub-DLAs and weaker LLSs are probably the systems that arise in massive spiral/elliptical galaxies.

The question remains: how do the single-cloud weak Mg II absorbers develop such high metallicities even at redshifts as high as $z \sim 1.7$? We know that the lines of sight that pass through these objects have $N_{\rm H\,I}$ 5 or 6 orders of magnitude below the star formation threshold. We also know that most single-cloud weak Mg II absorbers are not located very close to luminous galaxies, but that they tend to be in the vicinity (Churchill et al. 2005; Milutinović et al. 2006). Outflowing gas from dwarf galaxies in the local universe (e.g., Stocke et al. 2004) or from Lyman break galaxies at higher redshift (e.g., Adelberger et al. 2005) could partially contribute to the high metallicities in single-cloud weak Mg II systems. Schaye et al. (2007) have argued that high-metallicity intergalactic C IV clouds may be ejected as small clumps in superwinds from star-forming galaxies. However, at least some of the very high metallicity single-cloud weak Mg II absorbers show signs of Fe II line detections (e.g., our system 1 and several

systems in Rigby et al. 2002), although sometimes it is detected with only a few $\sigma$ level. For those systems, it has been stated that they are not $\alpha$-enhanced and that in situ star formation, including the less energetic Type Ia SNe that increase the iron to magnesium ratio, is responsible for enriching the gas (Rigby et al. 2002). Here readers should be aware that it is not the gas along the weak Mg II absorber line of sight that has formed stars, since it has much too low a column density. It must instead be a nearby molecular cloud region that was actively star-forming more than 1 billion years before the time from which we observe the absorber. That region would itself produce DLA absorption if a line of sight passed through it. It is known that many DLAs at $z < 1$ are associated only with dwarf or low surface brightness galaxies (Rao et al. 2003) and that in at least one case no galaxy is detected in deep narrowband H$\alpha$ images (Bouché et al. 2001).

So then why do DLAs not have high metallicities as well? And how do we explain the general trend of increasing metallicity with decreasing $N_{\rm H\,I}$? The reason could be simple. Large quantities of metals can be produced in star-forming regions in a variety of environments, inside and outside of galaxies. However, the metals will be dispersed into widely different types of regions, depending on the environment. Within giant galaxies molecular cloud regions are typically surrounded by a significant volume of high-density, high column density gas. So the metallicity is diminished by a large dilution effect as the ejected metals are spread through the galaxy region. In an intergalactic star-forming region, which is metal polluted by in situ star formation or has been ejected from a nearby dwarf galaxy, the clouds may not have a significant volume of high column density gas around it, and thus the dilution could be minimal. This would especially apply in a shallow potential well, where much of the surrounding gas is ejected by the early Type II SNe, and the remnant low-density gas remaining is greatly enhanced by the metals produced by later Type Ia's, which encounter a relatively sparse surrounding medium. The same type of dilution effect could lead to DLAs having lower metallicity than sub-DLAs. Prochaska et al. (2006) suggests that the supersolar metallicity sub-DLAs that they observed at $z \sim 1.7$, extreme members of the sub-DLA population, are related to regions affected by the feedback from actively star-forming regions. The metals would be spread to larger lower density sub-DLA regions by energetic processes.

Obviously, the metallicity of a region is determined by a combination of the amount of star formation activity in its vicinity and the overall density of its gas. In the case of the single-cloud weak Mg II absorbers, we conclude that the density effect dominates, leading to unexpected patches of high metallicity outside of galaxies. In the contrasting case of a DLA, there is just too much gas around it to dilute the metals coming through it, and a low metallicity often results.

REFERENCES

Adelberger, K. L., Shapley, A. E., Steidel, C. C., Pettini, M., Erb, D. K., & Reddy, N. A. 2005, ApJ, 629, 636
Akerman, C. J., Ellison, S. L., Pettini, M., & Steidel, C. C. 2005, A&A, 440, 499
Bergeron, J., & Boissé, P. 1991, A&A, 243, 344

Boisse, P., Le Brun, V., Bergeron, J., & Deharveng, J.-M. 1998, A&A, 333, 841
Bouché, N., Lowenthal, J. D., Charlton, J. C., Bershady, M. A., Churchill, C. W., & Steidel, C. C. 2001, ApJ, 550, 585
Bouché, N., Murphy, M. T., Péroux, C., Csabai, I., & Wild, V. 2006, MNRAS, 371, 495

Charlton, J. C., Ding, J., Zonak, S. G., Churchill, C. W., Bond, N. A., & Rigby, J. R. 2003, ApJ, 589, 111

Chen, H.-W., Kennicutt, R. C., Jr., & Rauch, M. 2005, ApJ, 620, 703

Churchill, C. W., & Charlton, J. C. 1999, AJ, 118, 59

Churchill, C. W., Kacprzak, G. G., & Steidel, C. C. 2005, in IAU Colloq. 199, Probing Galaxies through Quasar Absorption Lines, ed. P. R. Williams, C.-G. Shu, & B. Menard (Cambridge: Cambridge Univ. Press), 24

Churchill, C. W., Vogt, S. S., & Charlton, J. C. 2003, AJ, 125, 98

Cowie, L. L., & Songaila, A. 1998, Nature, 394, 44

Cowie, L. L., Songaila, A., Kim, T.-S., & Hu, E. M. 1995, AJ, 109, 1522

de la Varga, A., Reimers, D., Tytler, D., Barlow, T., & Burles, S. 2000, A&A, 363, 69

Ding, J., Charlton, J. C., & Churchill, C. W. 2005, ApJ, 621, 615

Ding, J., Charlton, J. C., Churchill, C. W., & Palma, C. 2003, ApJ, 590, 746

Djorgovski, S. G., et al. 2004, in ASP Conf. Ser. 312, Third Rome Workshop on Gamma-Ray Bursts in the Afterglow Era, ed. M. Feroci, F. Frontera, N. Masetti, & L. Piro (San Francisco: ASP), 249

Ellison, S. L., Hall, P. B., & Lira, P. 2005a, AJ, 130, 1345

Ellison, S. L., Kewley, L. J., & Mallén-Ornelas, G. 2005b, MNRAS, 357, 354

Ellison, S. L., Yan, L., Hook, I. M., Pettini, M., Wall, J. V., & Shaver, P. 2001, A&A, 379, 393

Erb, D. K., Shapley, A. E., Pettini, M., Steidel, C. C., Reddy, N. A., & Adelberger, K. L. 2006, ApJ, 644, 813

Fall, S. M., & Pei, Y. C. 1993, ApJ, 402, 479

Ferland, G., Korista, K. T., Verner, D. A., Ferguson, J. W., Kingdon, J. B., & Verner, E., M. 1998, PASP, 110, 761

Gabel, J. R., Arav, N., & Kim, T.-S. 2006, ApJ, 646, 742

Haardt, F., & Madau, P. 1996, ApJ, 461, 20

———. 2001, preprint (astro-ph/0106018v1)

Hamann, F., Barlow, T. A., Junkkarinen, V., & Burbidge, E. M. 1997, ApJ, 478, 80

Khare, P., Kulkarni, V. P., Lauroesch, J. T., York, D. G., Crotts, A. P. S., & Nakamura, O. 2004, ApJ, 616, 86

Khare, P., Kulkarni, V. P., Péroux, C., York, D. G., Lauroesch, J. T., & Meiring, J. D. 2007, A&A, 464, 487

Kulkarni, V. P., Fall, S. M., Lauroesch, J. T., York, D. G., Welty, D. E., Khare, P., & Truran, J. W. 2005, ApJ, 618, 68

Kulkarni, V. P., Khare, P., Péroux, C., York, D. G., Lauroesch, J. T., & Meiring, J. D. 2007, ApJ, 661, 88

Lanzetta, K. M., Wolfe, A. M., & Turnshek, D. A. 1995, ApJ, 440, 435

Lehner, N., Sembach, K. R., Dufton, P. L., Rolleston, W. R. J., & Keenan, F. P. 2001, ApJ, 551, 781

Lu, L., Sargent, W. L. W., Barlow, T. A., & Rauch, M. 1998, preprint (astro-ph/9802189)

Lynch, R. S., & Charlton, J. C. 2007, ApJ, 666, 64

Lynch, R. S., Charlton, J. C., & Kim, T.-S. 2006, ApJ, 640, 81

Mac Low, M.-M., & Ferrara, A. 1999, ApJ, 513, 142

Madau, P., Pozzetti, L., & Dickinson, M. 1998, ApJ, 498, 106

Masiero, J. R., Charlton, J. C., Ding, J., Churchill, C. W., & Kacprzak, G. 2005, ApJ, 623, 57

Meiring, J. D., et al. 2006, MNRAS, 370, 43

Milutinović, N., Rigby, J. R., Masiero, J. R., Lynch, R. S., Palma, C., & Charlton, J. C. 2006, ApJ, 641, 190

Narayanan, A., Charlton, J. C., Masiero, J. R., & Lynch, R. 2005, ApJ, 632, 92

Narayanan, A., Misawa, T., Charlton, J. C., & Kim, T.-S. 2007, ApJ, 660, 1093

Péroux, C., Dessauges-Zavadsky, M., D'Odorico, S., Kim, T.-S., & McMahon, R. G. 2003, MNRAS, 345, 480

Péroux, C., Kulkarni, V. P., Meiring, J., Ferlet, R., Khare, P., Lauroesch, J. T., Vladilo, G., & York, D. G. 2006a, A&A, 450, 53

Péroux, C., Meiring, J. D., Kulkarni, V. P., Ferlet, R., Khare, P., Lauroesch, J. T., Vladilo, G., & York, D. G. 2006b, MNRAS, 372, 369

Pettini, M., Ellison, S. L., Bergeron, J., & Petitjean, P. 2002, A&A, 391, 21

Pettini, M., Ellison, S. L., Steidel, C. C., & Bowen, D. V. 1999, ApJ, 510, 576

Pettini, M., Ellison, S. L., Steidel, C. C., Shapley, A. E., & Bowen, D. V. 2000, ApJ, 532, 65

Pettini, M., Smith, L. J., Hunstead, R. W., & King, D. L. 1994, ApJ, 426, 79

Pettini, M., Smith, L. J., King, D. L., & Hunstead, R. W. 1997, ApJ, 486, 665

Prochaska, J. X., & Burles, S. M. 1999, AJ, 117, 1957

Prochaska, J. X., Gawiser, E., Wolfe, A. M., Castro, S., & Djorgovski, S. G. 2003, ApJ, 595, L9

Prochaska, J. X., O'Meara, J. M., Herbert-Fort, S., Burles, S., Prochter, G. E., & Bernstein, R. A. 2006, ApJ, 648, L97

Prochaska, J. X., & Wolfe, A. M. 2000, ApJ, 533, L5

Rao, S. M., Nestor, D. B., Turnshek, D. A., Lane, W. M., Monier, E. M., & Bergeron, J. 2003, ApJ, 595, 94

Rigby, J. R., Charlton, J. C., & Churchill, C. W. 2002, ApJ, 565, 743

Russel, S. C., & Dopita, M. A. 1992, ApJ, 384, 508

Savaglio, S., et al. 2005, ApJ, 635, 260

Schaerer, D., & de Koter, A. 1997, A&A, 322, 598

Schaye, J., Carswell, R. F., & Kim, T.-S. 2007, MNRAS, 379, 1169

Somerville, R. S., Primack, J. R., & Faber, S. M. 2001, MNRAS, 320, 504

Songaila, A., & Cowie, L. L. 1996, AJ, 112, 335

Spite, M., et al. 2005, A&A, 430, 655

Stocke, J. T., Keeney, B. A., McLin, K. M., Rosenberg, J. L., Weymann, R. J., & Giroux, M. L. 2004, ApJ, 609, 94

Storrie-Lombardi, L. J., & Wolfe, A. M. 2000, ApJ, 543, 552

Tremonti, C. A., et al. 2004, ApJ, 613, 898

Tytler, D., Fan, X.-M., Burles, S., Cottrell, L., Davis, C., Kirkman, D., & Zuo, L. 1995, QSO Absorption Lines, ed. G. Meylan (New York: Springer), 289

Vladilo, G., & Péroux, C. 2005, A&A, 444, 461

Wolfe, A. M., Gawiser, E., & Prochaska, J. X. 2003, ApJ, 593, 235

York, D. G., et al. 2006, MNRAS, 367, 945

Zonak, S. G., Charlton, J. C., Ding, J., & Churchill, C. W. 2004, ApJ, 606, 196